J. Mech. Phys. Solids 205 (2025) 106330

Contents lists available at ScienceDirect

Journal of the Mechanics and Physics of Solids

journal homepage: www.elsevier.com/locate/jmps

The frictionless flexible sliding sleeve

Sebastien Neukirch [a], Francesco Dal Corso [b,*], Yury Vetyukov [c,*]

[a] Sorbonne Université, CNRS, Institut Jean Le Rond d'Alembert, F-75005 Paris, France
[b] DICAM, University of Trento, via Mesiano 77, I-38123 Trento, Italy
[c] Technische Universitaet Wien, Getreidemarkt 9, 1060 Vienna, Austria

ARTICLE INFO

Keywords:
Planar elastica
Variable-length structures
Configurational mechanics
Moving-boundary problems
Rod-to-rod contact

ABSTRACT

The planar mechanics of an elastic rod constrained by a frictionless, flexible sliding sleeve is analyzed. A variational approach is first applied to the equilibrium of an equivalent compound rod system with variable length, leading to a nonlinear boundary value problem. The equilibrium equations determine the deformation kinematics and, through a frictionless sliding condition governed by the Hamiltonian invariant, specify the overlapping length, but they do not reveal interaction forces between the flexible rod and the flexible sliding sleeve. To capture the interaction in detail, the system is modeled as two sub-rods, and both variational and micromechanical methods are employed independently, yielding identical closed-form expressions for the internal forces and moments within the overlapping region. This analysis reveals the presence of tangential concentrated interaction forces of repulsive nature at both ends of the overlapping region. The investigation is complemented by the numerical solution of four case studies, illustrating the broad mechanical behavior of the flexible, frictionless sleeve system. It is found that two different mechanisms may define the maximum bearing capacity, associated with the reciprocal ejection of the two sub-rods: either (i) a quasi-static disappearance of the overlap or (ii) a snap-through instability. The study also shows the possible vanishing of the distributed interaction force, even in non-symmetric configurations. This research establishes a novel theoretical framework for the mechanics of deployable systems and offers insights to advance the design and analysis of structures in fields such as aerospace, robotics, and civil and mechanical engineering.

1. Introduction

Highly deployable structures are functional systems designed for advanced applications that require fast assembly and disassembly. These structures stand out for their ease of transportation, as their disassembled form occupies significantly less volume compared to their operational dimensions (Pellegrino, 2001; Miura and Pellegrino, 2020). Traditionally, deployable structures have primarily addressed temporary construction needs, such as portable bridges, emergency shelters, mobile healthcare units, and space exploration. In recent years, they have also emerged as a vital concept in the development of innovative actuation mechanisms. In addition to the well-established categories of tensegrity (Micheletti and Podio-Guidugli, 2022) and origami (Misseroni et al., 2024) structures, another significant group of deployable structures based on sliding mechanisms is gaining recognition nowadays. To date, this group of structural systems has found applications in oil well drilling (Downton, 2007; Wicks et al., 2008; Fang et al., 2013; Denoël and Detournay, 2011), packing (Napoli and Turzi, 2015; Napoli and Goriely, 2017; Lombardo et al., 2018), robotics (Cicconofri and DeSimone, 2015; Gilbert et al., 2016; Renda et al., 2021; Alkayas et al., 2023; Alfalahi et al., 2020;

* Corresponding authors.
E-mail addresses: francesco.dalcorso@unitn.it (F. Dal Corso), yury.vetyukov@tuwien.ac.at (Y. Vetyukov).

https://doi.org/10.1016/j.jmps.2025.106330
Received 2 May 2025; Received in revised form 1 July 2025; Accepted 20 August 2025
Available online 27 August 2025

Boyer et al., 2022; Tong et al., 2025), and surgery (Duriez et al., 2006; Piskarev et al., 2024; Straathof et al., 2024; Liu and Chen, 2013b,a; Mao et al., 2024; Tummers et al., 2024). These systems can dramatically change their effective size or operational capabilities through relative sliding motions among their components or along external constraints. Consequently, the modeling of these structural systems involves contact mechanics and variable domains.

State of the art. Even within an elastic framework, the treatment of structural problems involving contact with obstacles can be quite challenging, particularly when the obstacle is deformable. Unilateral contact is typically addressed using a variational approach under an inequality constraint since the elastic beam may detach from the obstacle. In the case of an elastic beam constrained by a frictionless sliding sleeve, the problem simplifies as the contact constraint becomes an equality, although defined along an unknown contact region.

In the last decade, a research effort has been dedicated to investigating the mechanics of rods constrained by frictionless sliding sleeves that are rigid, namely highly stiff with respect to the constrained flexible element. It has been shown that the possible variation in the overlapping length introduces an unexpected non-zero tangential reaction at the entrance of the frictionless sleeve, associated with the curvature jump localized at that point (Bigoni et al., 2015). Such a force is nonlinear and has an outward direction, and has been exploited over the years to design mechanisms for: (i.) actuation for torsional (Bigoni et al., 2014b), serpentine (Dal Corso et al., 2017), and soft robotics locomotion (Cazzolli and Dal Corso, 2024); (ii.) buckling (Liakou and Detournay, 2018); (iii.) trivial path restabilization (Bigoni et al., 2014a; Bosi et al., 2016); (iv.) blistering (Goldberg and O'Reilly, 2022; Wang and Detournay, 2022); and (v.) self-tuning resonance (Koutsogiannakis et al., 2023; Migliaccio et al., 2025).

This non-zero tangential reaction finds a strong connection with configurational forces (Eshelby, 1951, 1956) and also inspired a Newtonian interpretation of the latter concept in fracture mechanics (Ballarini and Royer-Carfagni, 2016). With regard to such a connection, it is worth to highlight that the concept of configurational force (Gurtin, 1999; O'Reilly, 2017; Podio-Guidugli, 2001; Hanna et al., 2018; Singh and Hanna, 2021) is different from that of Newtonian force, therefore these two types of forces cannot be interchanged under a generic setting. Nevertheless, in special cases, the configurational force of a system may also take a value coincident with that of the tangential (Newtonian) reaction at the corner of a sliding sleeve exit, as in the frictionless contact of hyperelastic solids (Dal Corso et al., 2024).

Various Arbitrary Lagrangian–Eulerian (ALE) schemes and finite element formulations have recently been proposed to serve as efficient numerical tools for addressing mechanical problems involving frictionless sliding sleeve constraints (Han, 2023; Han and Bauchau, 2023; Vetyukov, 2024; Koutsogiannakis et al., 2025); see also the review paper (Scheidl and Vetyukov, 2023) for a general discussion of approaches towards solving problems with moving boundaries in structural mechanics.

Article contribution. We extend the planar analysis of elastic rods constrained by frictionless sliding sleeves to cases where both the constraint and constrained elements exhibit flexibility. The system under consideration can then be regarded as two inextensible and unshearable elastic sub-rods in reciprocal, frictionless bilateral contact along an overlapping region. Consequently, since each sub-rod is slender and modeled as a one-dimensional continuum along its center-line axis, both assume an abstractly coincident role, regardless of whether they physically represent the flexible sliding sleeve or the inserted flexible rod. By modeling the frictionless sliding sleeve system as a compound rod with variable length, we derive its equilibrium configuration in terms of kinematics of deformation and length of overlapping region by applying a variational approach. This results into a non-linear boundary value problem with an additional frictionless sliding condition. Despite its convenience, however, this approach does not provide a complete picture of the mechanics of the system. Indeed, as in the case of a rigid sleeve, discontinuities in internal forces and moments within each sub-rod arise at the end points of the contact (overlapping) region, which we henceforth refer to as transition points. These jumps correspond to concentrated forces and moments at these locations, representing the interaction between the two sub-rods. Similar to the rigid sleeve case, the concentrated interaction forces have a nonzero axial (namely, tangential) component, now governed by the bending stiffness of both sub-rods. Moreover, since both sub-rods are deformable, their interaction extends throughout the entire overlapping region, found to manifest exclusively as a normal contact force distribution. Through variational and micromechanical approaches (where in the latter we analyze the contact mechanics at the transition point in the presence of a small clearance), we derive explicit closed-form expressions to evaluate both the concentrated and distributed interaction forces, and we detail how the axial and shear components of the internal forces, as well as the internal moments, are split in each of the two sub-rods in the overlapping region.

Moreover, in the absence of distributed external loadings (such as gravity), we demonstrate that the Hamiltonian remains constant for each of the two sub-rods comprising the flexible frictionless sliding sleeve system. Consequently, no discontinuity in the Hamiltonian occurs at the transition point, despite the presence of concentrated interaction forces and moments, nor does it vary along the overlapping region. Considering that the Hamiltonian definition can be extended to the case of gravity (O'Reilly, 2015, 2017) and of other conservative loading (Neukirch and Bertails-Descoubes, 2025), we conjecture that the major results of the present work would hold in these cases.

Article outline. Without loss of generality, we address the specific problem of a simply supported flexible frictionless sliding sleeve, where the two supports remain at a fixed distance. The external loading condition consists of two concentrated moments applied at the supports. In Section 2, we solve this system under the linearized geometry approximation, considering both symmetric and generic configurations. In Section 3, we briefly recall the geometrically nonlinear framework of planar elastica and introduce key notations and fundamental quantities. Section 4 presents a variational approach in which the system is divided into three distinct regions, with the overlapping region treated as a compound structure consisting of two beams. In Section 5, by deriving the interaction concentrated and distributed forces, we examine how internal forces and moments are distributed between the

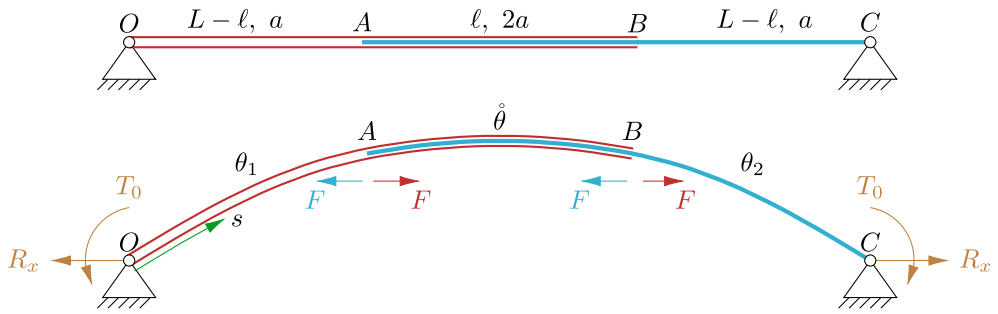

Fig. 1. Geometrically linear bending problem for a simply supported compound beam, loaded by a pair of moments T_0. (Top) The undeformed configuration ($T_0 = 0$). (Bottom) As T_0 is increased while the points O and C are kept fixed, relative frictionless sliding is occurring in the overlapping region AB and a reaction force R_x builds up at the supported ends.

two beams within the compound system. In Section 6, we present a simple numerical code, based on the derived theoretical solution, to compute equilibrium states and interaction forces. This solver is applied to four distinct case studies, illustrating the broad mechanical behavior of the flexible, frictionless sleeve system. Among the key findings, the analysis identifies two possible mechanisms for achieving maximum bearing capacity: either through the quasi-static disappearance of the overlapping length or the emergence of snap-through instability. Additionally, the study highlights the potential for complete annihilation of the distributed normal interaction force, even in a non-symmetric configuration. Finally, conclusions are drawn in Section 7.

Article significance. Building on the previous knowledge of variable-length systems constrained by rigid sliding sleeves, the present results extend the theoretical framework to structures where both the constraint and constrained elements are flexible. We enhance mechanical modeling approaches for deployable systems and provide insight into the distribution of internal forces and moments. The present comprehensive understanding of the interaction between flexible components can drive the optimization of mechanical performance, the enhancement of structural adaptability, and the overall improvement of system efficiency. The developed framework allows significant potential advancements in the design and analysis of deployable structures with aerospace, robotics, and mechanical and civil engineering applications.

2. A preliminary analysis in the geometrically linear setup

2.1. The symmetric case

We begin the investigation with a simple illustrative problem, which allows to introduce the basic notions and to demonstrate the effects, studied later in a more general setting. Consider a compound beam loaded by two moments at the simply supported ends, Fig. 1.

The structure comprises two sub-rods, the left one being a flexible sliding sleeve for the right one, as the latter is partially inside in the former. In the overlapping region, that is between the transition points A and B, sliding is realized without friction. The left and right supports are respectively at points O and C. For the simplicity of analytic treatment, in this Section we assume geometric linearity, and begin the analysis with a symmetric setup: both sub-rods possess the same mechanical properties, namely same bending stiffness a (we use this notation instead of the classical EI used in Strength of Materials texts) and same length L. Two external bending moments T_0 act on the rods at the supports in such a way that the bending direction is upwards. The length of the overlapping region ℓ is a configurational parameter, constrained within the set $\ell \in (0, L)$, which is defined by the fixed distance D between the two supports. Horizontal reaction forces R_x act on the structure by the supports at the ends. In the absence of friction, these forces are balanced by the horizontal component F of the interaction force between the sub-rods at the transition points, which we aim to determine.

We consider a compound rod with piecewise constant bending stiffness with the purpose of computing its total potential energy as a function of ℓ. Placing the origin of the material coordinate s at the left end in the point O, we denote by $y(s)$ the deflection and by $\theta(s) = y'(s)$ the angle of rotation of particles within three domains:

- left segment $0 < s < s_A$, bending stiffness a, $\theta = \theta_1$;
- overlapping segment $s_A < s < s_B$, bending stiffness $2a$, $\theta = \mathring{\theta}$;
- right segment $s_B < s < s_C$, bending stiffness a, $\theta = \theta_2$;

with

$$s_A = L - \ell, \quad s_B = L, \quad s_C = 2L - \ell. \tag{1}$$

Here, and in the following, we use a small ring as in $\mathring{\theta}$ to refer to a function defined in the overlapping region. Because $\theta(s)$ is continuous, the three functions must match in the transition points:

$$\theta_1(s_A) = \mathring{\theta}(s_A), \quad \mathring{\theta}(s_B) = \theta_2(s_B). \tag{2}$$

The bending moment $M = -T_0$ (according to the sign convention) is constant as there are no vertical forces in the supports and the deflections are small.[1] The constitutive relations read

$$a\,\theta_1' = M, \quad 2\,a\,\mathring{\theta}' = M, \quad a\,\theta_2' = M. \tag{3}$$

Using the symmetry of the problem, it is easy to integrate the equations piecewise and to obtain the strain energy and the potential of external loads. Moreover, the statical determinacy of the problem makes it even easier to compute the total complementary strain energy, whose density is known in all three segments. This equals the strain energy $\mathcal{E}$ itself because of the linearity of the problem and reads

$$\mathcal{E} = \frac{M^2}{2a} s_A + \frac{M^2}{4a}(s_B - s_A) + \frac{M^2}{2a}(s_C - s_B), \tag{4}$$

which, by considering the coordinate values given in Eq. (1), reduces to

$$\mathcal{E}(\ell) = \frac{M^2}{4a}(4L - 3\ell). \tag{5}$$

According to Clapeyron's theorem, the work of external load $\mathcal{W}$ is twice the elastic energy, $\mathcal{W} = 2\mathcal{E}$, and the total potential energy $\mathcal{V} = \mathcal{E} - \mathcal{W}$ reduces to

$$\mathcal{V}(\ell) = -\mathcal{E}(\ell) = \frac{M^2}{4a}(3\ell - 4L). \tag{6}$$

The energy decreases as the length of the overlapping region becomes smaller, which means the rod would slide out of the sleeve given the freedom to do so, i.e. if one of the supports would be movable horizontally. Here, the end-to-end distance OC is fixed to $D(\ell) = 2L - \ell$ and the structure remains in equilibrium because of the reaction force R_x, which would become an active force needed to prevent sliding if the right support were movable. Considering the Lagrangian $\mathcal{L}$

$$\mathcal{L}(\ell) = \mathcal{V}(\ell) - R_x\, D(\ell), \tag{7}$$

the equilibrium is obtained by writing the stationarity condition

$$\frac{\partial \mathcal{L}(\ell)}{\partial \ell} = 0 \quad \Rightarrow \quad R_x = -\frac{\partial \mathcal{V}(\ell)}{\partial \ell}, \tag{8}$$

showing that (within a linear setting) *the horizontal reaction R_x is an Eshelby-like force for the system.*[2] By performing such a computation, it follows that

$$R_x = -\frac{3M^2}{4a}, \tag{9}$$

and therefore R_x has a negative value, realizing a compressive state in the flexible sleeve system. After obtaining the R_x value, it is also possible to evaluate the horizontal component F of the interaction force between the sub-rods at the transition points, see Fig. 1. Note that the forces at A and B are equal because of the symmetry and the assumed identical mechanical properties of the sub-rods. The horizontal equilibrium of each of them implies $2F = -R_x$, and thus the horizontal interaction force results in

$$F = \frac{3M^2}{8a}. \tag{10}$$

This deviates from the known value $M^2/(2a)$, which holds in the case of a rigid sleeve (Bigoni et al., 2015). This specific result Eq. (10) was easy to obtain owing to the symmetry and linearity of the problem. Furthermore, we ignored small but potentially important horizontal components of the transverse contact concentrated and distributed forces between the sub-rods, as their resultants vanish because of the symmetry of the setup. In the following we demonstrate that, in a general nonsymmetric case, this higher-order effect has to be accounted for to again arrive at Eq. (10), making computations more complicated. More advanced argumentation featuring the small extensibility of the rods will need to be invoked to compute the tangential contact force in the more general case of nonsymmetric large deformations with possible differences in the rigidities of the sub-rods.

2.2. The nonsymmetric case

We now consider the case where the structure of Fig. 1 is loaded with two different external torques T_l and T_r, and the two sub-rods may have different bending stiffnesses a_1 and a_2. The end-to-end distance OC is still fixed to $D(\ell) = 2L - \ell$ and in the

[1] See Fig. 8 below for the evolution of the deformation of the structure with increasing external moment T_0 in the geometrically nonlinear case, when the horizontal reaction forces in the supports contribute to the bending moment distribution $M(s)$.

[2] The nomenclature *Eshelby-like* force has been first introduced in Bigoni et al. (2015) to highlight the strong connection of Newtonian forces with configurational ones in variable-length systems. More specifically, the reaction R_x of the present simply supported system with non-moving points O and C takes the value of the configurational force for the system, would the constraint at the point C be released to allow motion along x. This is analogous to the coincidence of the configurational force with the opposite of the tangential component of the concentrated reaction at the corner of a rigid flat punch in frictionless contact with an hyperelastic solids (Dal Corso et al., 2024).

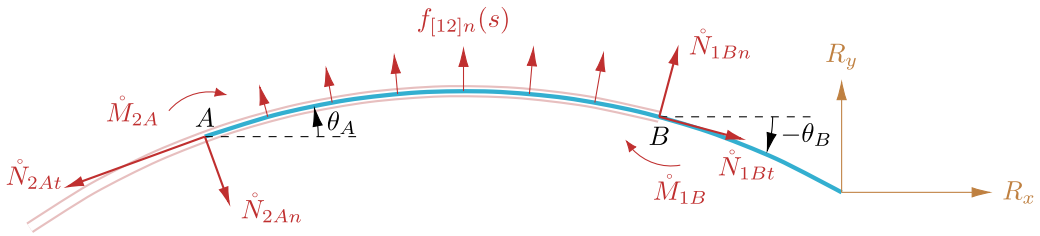

Fig. 2. Free-body diagram of sub-rod 2. The normal distributed load $f_{[12]n}(s)$ can be neglected in the equilibrium of the linearized case as providing higher-order contribution (see Section 5.2 for details, Eq. (89)).

present geometrically linear setup, we have that the horizontal x and vertical y positions at the arc length coordinate s are defined as

$$x(s) = s, \qquad y(s) = \int_0^s \theta(\sigma)\,\mathrm{d}\sigma, \qquad s \in [0, D]. \tag{11}$$

The internal moment M is no longer uniform $M(s,\ell) = -T_l - R_y(\ell)s$, and the reaction force $\boldsymbol{R}$ now has both horizontal R_x and vertical R_y components. The vertical component is obtained through a moment balance $R_y(\ell) = (T_r - T_l)/D(\ell)$, while the horizontal component is obtained by looking for the stationary point of the Lagrangian $\mathcal{L}$, which again provides *the horizontal reaction R_x as a configurational force for the system as expressed by Eq.* (8). Using again Clapeyron's theorem, we have $\mathcal{W}(\ell) = 2\mathcal{E}(\ell)$ and hence $\mathcal{V}(\ell) = -\mathcal{E}(\ell)$, which finally yields

$$R_x = \frac{\partial \mathcal{E}(\ell)}{\partial \ell} = -\frac{T_l^2}{a_1}\rho\left(\frac{a_2}{a_1}, \frac{T_r}{T_l}, \frac{\ell}{L}\right) < 0. \tag{12}$$

Here $\rho > 0$ is a dimensionless quantity, whose expression is reported in Appendix A, together with that of the elastic energy $\mathcal{E}(\ell)$. Eq. (12) generalizes to nonsymmetric flexible sleeve systems the result in Eq. (9) obtained for symmetric ones, and confirms that the horizontal reaction R_x is always compressive.

Considering the global force balance of sub-rod 2 (Fig. 2), we write the reaction force $\boldsymbol{R} = R_x\boldsymbol{e}_x + R_y\boldsymbol{e}_y$ as the following sum of force contributions

$$\begin{aligned} R_x &= \underbrace{\overbrace{\mathring{N}_{2At}}^{\sim\theta^2} - \overbrace{\mathring{N}_{2An}\theta_A}^{\sim\theta^2}}_{-F_{A[12]x}} + \underbrace{\overbrace{\mathring{N}_{1Bt}}^{\sim\theta^2} - \overbrace{\mathring{N}_{1Bn}\theta_B}^{\sim\theta^2}}_{-F_{B[12]x}} - \overbrace{\int_{L-\ell}^{L} f_{[12]n}(s)\theta(s)\,\mathrm{d}s}^{\sim\theta^4}, \\ R_y &= \underbrace{\overbrace{\cancel{\mathring{N}_{2At}\theta_A}}^{\sim\theta^3} + \overbrace{\mathring{N}_{2An}}^{\sim\theta}}_{-F_{A[12]y}} + \underbrace{\overbrace{\cancel{\mathring{N}_{1Bt}\theta_B}}^{\sim\theta^3} + \overbrace{\mathring{N}_{1Bn}}^{\sim\theta}}_{-F_{B[12]y}} - \overbrace{\int_{L-\ell}^{L} f_{[12]n}(s)\,\mathrm{d}s}^{\sim\theta^3}, \end{aligned} \tag{13}$$

the first two terms being the concentrated force coming from sub-rod 1 at point A, the two subsequent terms being the concentrated force coming from sub-rod 1 at point B, and the last term being the distributed force coming from sub-rod 1 in the overlapping region, see Eq. (93). As it will be explained in Section 5, these terms scale in different manners with the global deflection of the structure and in the present small deflection limit, we see that only the forces at the transition points A and B matter (the corresponding order is highlighted above the terms in Eq. (13)).

It is finally observed that in the symmetric case of Section 2.1 ($a_1 = a_2 = a$, $T_r = T_l = T_0$), we find $R_y(\ell) = 0$, $\rho = 3/4$ and

$$R_x = -\frac{3T_0^2}{4a}, \quad \mathring{N}_{2At} = \mathring{N}_{1Bt} = \frac{R_x}{2} = -\frac{3T_0^2}{8a}, \quad \mathring{N}_{2An} = \mathring{N}_{1Bn} = \frac{R_y}{2} = 0, \quad \theta_B = -\theta_A, \quad \theta_B' = \theta_A', \tag{14}$$

and therefore

$$F_{A[12]x} = F_{B[12]x} = \frac{3T_0^2}{8a}, \quad F_{A[12]y} = F_{B[12]y} = 0. \tag{15}$$

3. Nonlinear model for the planar mechanics of flexible, inextensible, and unshearable rods

The subsequent analysis of the sliding sleeve problem is based on the relations of the geometrically nonlinear theory of rods under planar bending. In this section we consider the model of an inextensible, unshearable rod at finite rotations. Following (Antman, 2004; Goss, 2009; Bigoni, 2012; Vetyukov, 2014, 2012), we here refer to this problem as the planar elastica, define useful quantities, and recall equilibrium equations and some properties of the equilibrium solutions.

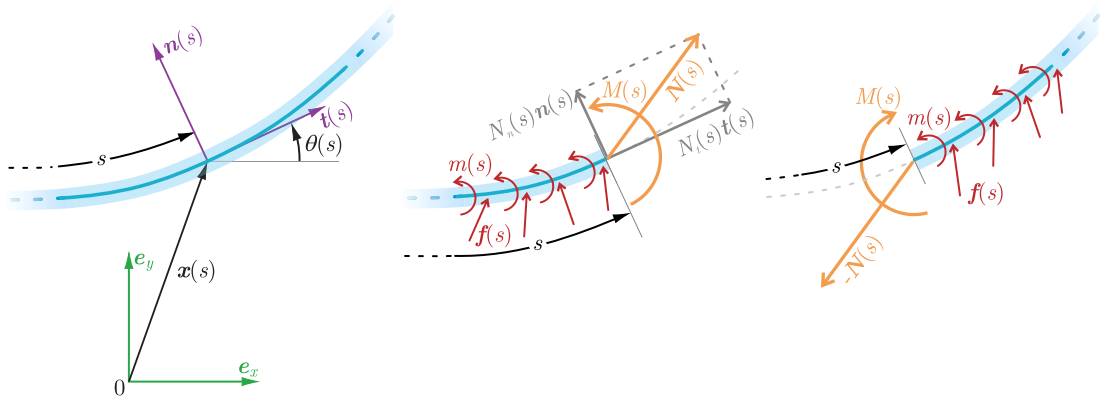

Fig. 3. In-plane kinematics and statics of an inextensible and unshearable rod. (Left) Global $\boldsymbol{e}_x$–$\boldsymbol{e}_y$ and local $\boldsymbol{t}(s)$–$\boldsymbol{n}(s)$ orthonormal bases. The deformed configuration is uniquely described by the inclination $\theta(s)$ of the rod axis at the curvilinear coordinate s with respect to $\boldsymbol{e}_x$. (Center and right) Internal moment $M(s)$ and internal force vector $\boldsymbol{N}(s)$, together with its components along the local orthonormal basis $\boldsymbol{t}(s)$–$\boldsymbol{n}(s)$. External distributed force $\boldsymbol{f}(s)$ and moment $m(s)$ are also shown.

3.1. Kinematics

We consider a rod that is straight in its undeformed state. In its deformed (current) planar configuration, the rod axis is described by the position vector $\boldsymbol{x}(s) = x(s)\boldsymbol{e}_x + y(s)\boldsymbol{e}_y$, as a function of the curvilinear (arc-length) coordinate s, with $\boldsymbol{e}_x$ and $\boldsymbol{e}_y$ being the orthonormal Cartesian basis for the deformation plane (Fig. 3, left). As the rod is inextensible, $|\mathrm{d}\boldsymbol{x}| = \mathrm{d}s$, the tangent vector $\boldsymbol{t}(s) = \boldsymbol{x}'(s)$ is given in term of the (positive when counter-clockwise) inclination $\theta(s)$ of the rod axis with respect to $\boldsymbol{e}_x$, namely

$$\boldsymbol{t}(s) = \cos\theta(s)\boldsymbol{e}_x + \sin\theta(s)\boldsymbol{e}_y. \tag{16}$$

For Kirchhoff rods, the angle $\theta(s)$ is coincident with the rotation angle of an oriented particle from the reference state due to the assumption of no shear deformability. By introducing with a prime the derivative with respect to the relevant arc-length coordinate s, the derivative $\boldsymbol{t}'(s)$ of the tangent vector is given by

$$\boldsymbol{t}'(s) = \theta'(s)\,\partial_\theta \boldsymbol{t} = \theta'(s)\,\boldsymbol{n}(s). \tag{17}$$

Here $\theta'(s)$ is the curvature and $\boldsymbol{n}(s)$ is the unit normal vector,

$$\boldsymbol{n}(s) = -\sin\theta(s)\boldsymbol{e}_x + \cos\theta(s)\boldsymbol{e}_y, \tag{18}$$

which is orthogonal to the tangent vector, $\boldsymbol{t}(s)\cdot\boldsymbol{n}(s) = 0$, and whose derivative satisfies $\boldsymbol{n}'(s) = -\theta'(s)\,\boldsymbol{t}(s)$.

3.2. Statics

The internal force vector $\boldsymbol{N}(s)$ stands for the force between the two neighboring particles of the rod at s. It is the force the particle at s^+ exerts on the particle at s^- (Fig. 3, center). It can be decomposed along the absolute orthonormal basis $\boldsymbol{e}_x$–$\boldsymbol{e}_y$ as $\boldsymbol{N}(s) = N_x(s)\,\boldsymbol{e}_x + N_y(s)\,\boldsymbol{e}_y$ and equivalently to the relative one $\boldsymbol{t}(s)$–$\boldsymbol{n}(s)$ as $\boldsymbol{N}(s) = N_t(s)\,\boldsymbol{t}(s) + N_n(s)\,\boldsymbol{n}(s)$, being $N_x(s)$ and $N_y(s)$ the Cartesian components and $N_t(s) = \boldsymbol{N}(s)\cdot\boldsymbol{t}(s)$ and $N_n(s) = \boldsymbol{N}(s)\cdot\boldsymbol{n}(s)$ the internal axial (or tension) and shear force, respectively. By introducing the internal bending moment $M(s)$ (Fig. 3, center), the equilibrium condition under the external distributed force $\boldsymbol{f}(s)$ and moment $m(s)$ is provided by the local balance equations

$$\boldsymbol{N}'(s) + \boldsymbol{f}(s) = 0, \tag{19a}$$

$$M'(s) + \boldsymbol{x}'(s)\times\boldsymbol{N}(s)\cdot\boldsymbol{e}_z + m(s) = 0, \tag{19b}$$

where $\boldsymbol{e}_z = \boldsymbol{e}_x\times\boldsymbol{e}_y = \boldsymbol{t}(s)\times\boldsymbol{n}(s)$. Due to the inextensibility assumption ($\boldsymbol{x}' = \boldsymbol{t}$), the scalar triple product property ($\boldsymbol{t}\times\boldsymbol{N}\cdot\boldsymbol{e}_z = \boldsymbol{e}_z\times\boldsymbol{t}\cdot\boldsymbol{N}$), and considering that $\boldsymbol{e}_z\times\boldsymbol{t} = \boldsymbol{n}$, the identity $\boldsymbol{x}'(s)\times\boldsymbol{N}(s)\cdot\boldsymbol{e}_z = \boldsymbol{N}(s)\cdot\boldsymbol{n}(s) = N_n(s)$ holds. By assuming a linear constitutive relation between the bending moment $M(s)$ and the curvature $\theta'(s)$ with a constant bending stiffness a,

$$M(s) = a\,\theta'(s), \tag{20}$$

the moment balance (19b) simplifies to

$$a\theta''(s) + N_n(s) + m(s) = 0. \tag{21}$$

Now that the basic equations of the theory of Kirchhoff rods are formulated, we establish some further relations, useful for the subsequent analysis. Considering that the derivatives of the internal axial $N_t(s)$ and shear $N_n(s)$ forces are respectively given by

$N_t'(s) = \boldsymbol{N}'(s)\cdot\boldsymbol{t}(s) + \boldsymbol{N}(s)\cdot\boldsymbol{t}'(s)$ and $N_n'(s) = \boldsymbol{N}'(s)\cdot\boldsymbol{n}(s) + \boldsymbol{N}(s)\cdot\boldsymbol{n}'(s)$, and decomposing the external distributed force $\boldsymbol{f}(s)$ into its normal and the tangent components, $\boldsymbol{f}(s) = f_t(s)\,\boldsymbol{t}(s) + f_n(s)\,\boldsymbol{n}(s)$, the balance of forces (19a) can be rewritten as

$$N_t'(s) = -f_t(s) + \theta'(s)N_n(s), \qquad N_n'(s) = -f_n(s) - \theta'(s)N_t(s). \tag{22}$$

3.3. Hamiltonian $\mathcal{H}(s)$ and its possible invariance

The product of the moment balance (21) with $\theta'(s)$ can be rewritten by considering Eq. $(22)_1$ as

$$\left(\frac{a}{2}\left(\theta'(s)\right)^2 + N_t(s)\right)' + f_t(s) + m(s)\theta'(s) = 0. \tag{23}$$

By introducing the quantity $\mathcal{H}(s)$ defined as

$$\mathcal{H}(s) = \frac{a}{2}\left(\theta'(s)\right)^2 + N_t(s), \qquad \text{or equivalently} \qquad \mathcal{H}(s) = \frac{M(s)^2}{2a} + N_t(s), \tag{24}$$

the integration of Eq. (23) over the finite interval with bounds s_A and s_B leads to

$$\mathcal{H}(s_B) - \mathcal{H}(s_A) = -\int_{s_A}^{s_B}\left[f_t(s) + m(s)\theta'(s)\right]\mathrm{d}s. \tag{25}$$

Eq. (25) shows that the quantity $\mathcal{H}(s)$ is conserved

$$\mathcal{H}(s) = \mathcal{H}, \tag{26}$$

whenever the integral condition $\int_{s_A}^{s_B}\left[f_t(s) + m(s)\theta'(s)\right]\mathrm{d}s = 0$ holds for every pair of s_A and s_B, and therefore when the tangential component $f_t(s)$ and the moment $m(s)$ satisfy

$$f_t(s) + m(s)\theta'(s) = 0, \tag{27}$$

including the case where both functions identically vanish, $f_t(s) = m(s) = 0$. Under this circumstance, the quantity $\mathcal{H}$ is called the *Hamiltonian invariant* (Dichmann et al., 1996; Kehrbaum and Maddocks, 1997; Nizette and Goriely, 1999).

Discontinuity due to concentrated forces. The case of a concentrated external force $\boldsymbol{F}_0$ and moment M_0 applied at the curvilinear coordinate s_0 can be addressed by exploiting (25) under external distributed force and moment respectively given by $\boldsymbol{f}(s) = \boldsymbol{F}_0\,\delta(s - s_0)$ and $m(s) = M_0\,\delta(s - s_0)$ and the bounds as $s_A = s_0^-$ and $s_B = s_0^+$. This leads to the jump condition (O'Reilly, 2017)

$$[\![\mathcal{H}(s_0)]\!] = -F_{0t} - M_0\left\langle\theta'(s_0)\right\rangle, \tag{28}$$

where F_{0t} is the axial component of the concentrated force $\boldsymbol{F}_0$, and the symbols $[\![\mathcal{H}(s_0)]\!]$ and $\langle\theta'(s_0)\rangle$ respectively stand for the jump and mean value of the relevant argument at the coordinate s_0,

$$[\![\mathcal{H}(s_0)]\!] = \mathcal{H}(s_0^+) - \mathcal{H}(s_0^-), \qquad \left\langle\theta'(s_0)\right\rangle = \frac{\theta'(s_0^-) + \theta'(s_0^+)}{2}. \tag{29}$$

It is noted that the integral of the product of a Dirac δ-function with discontinuous $\theta'(s)$ at s_0 does not automatically imply the form with the mean value. However, the jump condition (28) is obtained by integrating the moment balance (21) in a small vicinity around point s_0, provided the concentrated moment is replaced by a distributed one.

Furthermore, in analogy with the invariance of $\mathcal{H}$ obtained in the case of distributed loadings satisfying Eq. (27), the continuity of $\mathcal{H}$ is restored for a special combination of the tangential force component F_{0t} and the moment M_0 corresponding to

$$F_{0t} + M_0\left\langle\theta'(s_0)\right\rangle = 0 \qquad \Leftrightarrow \qquad [\![\mathcal{H}(s_0)]\!] = 0. \tag{30}$$

Discontinuity due to bending stiffness jump. The Hamiltonian $\mathcal{H}$ has a discontinuity at the coordinate s_0 if the bending stiffness a jumps, $a(s_0^+) \neq a(s_0^-)$. In this case, although the axial force N_t and the moment M are both continuous at s_0 due to the absence of external loadings, a jump in the curvature $\theta'(s)$ is displayed, which in turn leads to a jump there in the Hamiltonian $\mathcal{H}$ (24). By recalling the constitutive relation (20), the jump of $\mathcal{H}$ at s_0 reduces to $[\![\mathcal{H}(s_0)]\!] = M(s_0)[\![\theta'(s_0)]\!]/2$. It is worth observing that such a jump value is consistent with the configurational (or material) force reported by Kienzler and Herrmann (1986), see their Eq. (24) and (25).

4. Equilibrium equations for the compound rod model

The large deformation of a flexible rod (sub-rod 2) partially inserted into a flexible sleeve (sub-rod 1) is depicted in Fig. 4. The bending stiffness of the sleeve equals a_1 and that of the rod equals a_2, such that the effective bending stiffness of the compound rod model in the overlapping region is $a_1 + a_2$. Changing the ratio a_1/a_2 from 1 to $+\infty$, we make a smooth transition from the symmetric setting to the classic case of a rigid sleeve. Unlike the simple example in Section 2, we now seek the equilibrium of the compound system in a geometrically nonlinear setup. Again, the single material coordinate s parametrizes the entire compound rod, whose both ends are hinged on the x axis with the size of the span $2L - \ell_0$, where ℓ_0 is the length of the overlapping region in

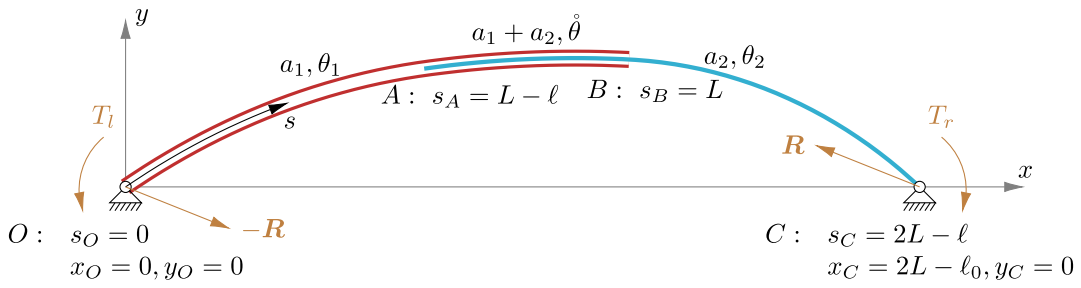

Fig. 4. Flexible rod (sub-rod 2, blue) partially inserted in a flexible sleeve (sub-rod 1, red) with transition points A and B and imposed distance between the two supports in O and C defined as $2L - \ell_0 > L$. The externally applied bending moments T_l and T_r, as well as the reaction forces $\boldsymbol{R}$ and $-\boldsymbol{R}$, are plotted at the hinged end points. The presented shape is the equilibrium solution for $a_1 = 1.5$, $a_2 = 1$, $L = 1$, $\ell_0 = 0.5$, and $T_l = T_r = 1$ (SI units) computed using the code presented in Fig. 7.

the unloaded (undeformed) state subject to $\ell_0 \in (0, L)$. For the quantities $x, y, \theta, \boldsymbol{N}, M, \boldsymbol{t}, \boldsymbol{n}$, we use the symbol $\mathring{g}(s)$ to denote for the generic function $g(s)$ in the overlapping region, and indices $g_1(s)$ or $g_2(s)$ refer to individual sub-rods.

The generic configuration of the inextensible compound rod with variable domain is described by the inclination $\theta(s)$ and the current overlapping length $\ell \in (0, L)$. Considering that the inclination $\theta(s)$ displays a first derivative jump at the points A and B, associated with the coordinates $s_A = L - \ell$ and $s_B = L$, it is instrumental to consider three continuous inclination functions, namely the two inclinations $\theta_1(s)$ and $\theta_2(s)$, respectively of sub-rod 1 and 2 outside the overlapping region, and the inclination $\mathring{\theta}(s)$ of the compound rod along the overlapping region, namely

$$\theta(s) = \begin{cases} \theta_1(s), & s \in [0, L - \ell], \\ \mathring{\theta}(s), & s \in [L - \ell, L], \\ \theta_2(s), & s \in [L, 2L - \ell]. \end{cases} \tag{31}$$

The flexible sleeve system can be interpreted as a compound inextensible rod with variable domains and a piecewise constant bending stiffness $a(s)$ having discontinuities located at the transition points A and B, namely

$$a(s) = \begin{cases} a_1, & s \in [0, L - \ell), \\ a_1 + a_2, & s \in (L - \ell, L), \\ a_2, & s \in (L, 2L - \ell], \end{cases} \tag{32}$$

from which the linear constitutive response (20) follows as

$$M(s) = \begin{cases} M_1(s) = a_1 \theta_1'(s), & s \in [0, L - \ell], \\ \mathring{M}(s) = (a_1 + a_2)\mathring{\theta}'(s), & s \in [L - \ell, L], \\ M_2(s) = a_2 \theta_2'(s), & s \in [L, 2L - \ell]. \end{cases} \tag{33}$$

A variational approach is used to derive the equations governing the equilibrium of the system. The total potential energy $\mathcal{V}$ is given by the difference between the bending elastic energy $\mathcal{E}$ and the work $\mathcal{W}$ done by the two end moments T_l and T_r (respectively at points O, $s = 0$, and C, $s = 2L - \ell$)

$$\mathcal{V} = \mathcal{E} - \mathcal{W}, \tag{34}$$

where $\mathcal{E} = \mathcal{E}_1 + \mathring{\mathcal{E}} + \mathcal{E}_2$, with

$$\mathcal{E}_1 = \frac{a_1}{2} \int_0^{L-\ell} \left(\theta_1'(s)\right)^2 \, \mathrm{d}s, \quad \mathring{\mathcal{E}} = \frac{a_1 + a_2}{2} \int_{L-\ell}^{L} \left(\mathring{\theta}'(s)\right)^2 \, \mathrm{d}s, \quad \mathcal{E}_2 = \frac{a_2}{2} \int_L^{2L-\ell} \left(\theta_2'(s)\right)^2 \, \mathrm{d}s, \tag{35}$$

and

$$\mathcal{W} = T_l \theta_1(0) - T_r \theta_2(2L - \ell). \tag{36}$$

The stationarity of the total potential energy $\mathcal{V}$ under the kinematic constraints

$$\begin{aligned} &d_A = \theta_1(L - \ell) - \mathring{\theta}(L - \ell) = 0, \\ &d_B = \mathring{\theta}(L) - \theta_2(L) = 0, \\ &\boldsymbol{d}_C = \int_0^{L-\ell} \boldsymbol{t}_1(s) \, \mathrm{d}s + \int_{L-\ell}^{L} \mathring{\boldsymbol{t}}(s) \, \mathrm{d}s + \int_L^{2L-\ell} \boldsymbol{t}_2(s) \, \mathrm{d}s - (2L - \ell_0)\boldsymbol{e}_x = \boldsymbol{0}, \end{aligned} \tag{37}$$

can be addressed by considering the Lagrangian $\mathcal{L}$,

$$\mathcal{L}\left(\theta_1(s), \mathring{\theta}(s), \theta_2(s), \ell\right) = \mathcal{V} - \mu_A \, d_A - \mu_B \, d_B - \boldsymbol{R} \cdot \boldsymbol{d}_C, \tag{38}$$

defined as the potential energy $\mathcal{V}$ enhanced by the presence of Lagrange multipliers μ_A and μ_B (representative of bending moment values at the respective cross-sections) and $\boldsymbol{R}$ (representative of the reaction force at the right support), respectively multiplied by the constraints d_A, d_B, and $\boldsymbol{d}_C$, representing 4 equivalent scalar constraints. The vectorial constraint $\boldsymbol{d}_C$ concerns the given relative position of the right end and comprises two scalar conditions, while the scalar constraints d_A and d_B respectively concern the continuity of the tangent vector at the points A and B,

$$\boldsymbol{t}_{1A} = \mathring{\boldsymbol{t}}_A, \qquad \boldsymbol{t}_{2B} = \mathring{\boldsymbol{t}}_B, \tag{39}$$

where the following symbology has been introduced (with reference to a generic function g)

$$g_{1A} = g_1(s = L - \ell), \qquad \mathring{g}_A = \mathring{g}(s = L - \ell), \qquad g_{2B} = g_2(s = L), \qquad \mathring{g}_B = \mathring{g}(s = L). \tag{40}$$

The equilibrium configurations for the system are associated with extrema of the Lagrangian $\mathcal{L}$, which implies that the first variation $\overline{\mathcal{L}}$

$$\overline{\mathcal{L}} = \overline{\mathcal{V}} - \mu_A \overline{d}_A - \mu_B \overline{d}_B - \boldsymbol{R} \cdot \overline{\boldsymbol{d}}_C, \tag{41}$$

(where the overbar stands for the variation of the relevant quantity) must vanish at all possible values of independent variations $\overline{\theta}_1(s)$, $\overline{\mathring{\theta}}(s)$, $\overline{\theta}_2(s)$, and $\overline{\ell}$. Through the Leibniz rule and integration by parts, the first variation $\overline{\mathcal{L}}$ is found to be

$$\begin{aligned}
\overline{\mathcal{L}} = \; & -\int_0^{L-\ell} \left[a_1\, \theta_1''(s) + \boldsymbol{R} \cdot \boldsymbol{n}_1(s)\right] \overline{\theta}_1(s)\, \mathrm{d}s - \int_{L-\ell}^{L} \left[(a_1 + a_2)\, \mathring{\theta}''(s) + \boldsymbol{R} \cdot \mathring{\boldsymbol{n}}(s)\right] \overline{\mathring{\theta}}(s)\, \mathrm{d}s - \int_L^{2L-\ell} \left[a_2\, \theta_2''(s) + \boldsymbol{R} \cdot \boldsymbol{n}_2(s)\right] \overline{\theta}_2(s)\, \mathrm{d}s \\
& - \left[a_1\, \theta_{1O}' + T_l\right] \overline{\theta}_{1O} + \left[a_1\, \theta_{1A}' - \mu_A\right] \overline{\theta}_{1A} - \left[(a_1 + a_2)\, \mathring{\theta}_A' - \mu_A\right] \overline{\mathring{\theta}}_A + \left[(a_1 + a_2)\, \mathring{\theta}_B' - \mu_B\right] \overline{\mathring{\theta}}_B - \left[a_2\, \theta_{2B}' - \mu_B\right] \overline{\theta}_{2B} \\
& + \left[a_2\, \theta_{2C}' + T_r\right] \overline{\theta}_{2C} + \left\{-\frac{1}{2}\left[a_1 \left(\theta_{1A}'\right)^2 - (a_1 + a_2) \left(\mathring{\theta}_A'\right)^2 + a_2 \left(\theta_{2C}'\right)^2\right] + \boldsymbol{R} \cdot \boldsymbol{t}_{2C} + \mu_A \left(\theta_{1A}' - \mathring{\theta}_A'\right) - T_r \theta_{2C}'\right\} \overline{\ell},
\end{aligned} \tag{42}$$

where, in addition to (40), the further symbology is also introduced (with reference to a generic function g)

$$g_{1O} = g_1(s = 0), \qquad g_{2C} = g_2(s = 2L - \ell). \tag{43}$$

Requiring the first variation $\overline{\mathcal{L}}$ to vanish for every variation $\overline{\theta}_1(s)$, $\overline{\mathring{\theta}}(s)$, and $\overline{\theta}_2(s)$ yields the nonlinear equilibrium equations, expressed by the celebrated elastic equations, for the compound system across the three regions

$$\begin{cases}
a_1\, \theta_1''(s) + N_{1n}(s) = 0, & s \in [0, L - \ell], \\
(a_1 + a_2)\, \mathring{\theta}''(s) + \mathring{N}_n(s) = 0, & s \in [L - \ell, L], \\
a_2\, \theta_2''(s) + N_{2n}(s) = 0, & s \in [L, 2L - \ell].
\end{cases} \tag{44}$$

Here

$$N_{1n}(s) = \boldsymbol{R} \cdot \boldsymbol{n}_1(s), \qquad \mathring{N}_n(s) = \boldsymbol{R} \cdot \mathring{\boldsymbol{n}}(s), \qquad N_{2n}(s) = \boldsymbol{R} \cdot \boldsymbol{n}_2(s), \tag{45}$$

together with the boundary conditions at the two end points O and C

$$a_1\, \theta_{1O}' = -T_l, \qquad a_2\, \theta_{2C}' = -T_r, \tag{46}$$

and the values of the Lagrange multipliers μ_A and μ_B

$$\mu_A = a_1\, \theta_{1A}' = (a_1 + a_2)\, \mathring{\theta}_A', \qquad \mu_B = (a_1 + a_2)\, \mathring{\theta}_B' = a_2\, \theta_{2B}', \tag{47}$$

confirming the curvature jumps at points A and B, namely,

$$\mathring{\theta}_A' = \frac{a_1}{a_1 + a_2}\, \theta_{1A}', \qquad \mathring{\theta}_B' = \frac{a_2}{a_1 + a_2}\, \theta_{2B}'. \tag{48}$$

Using (47) and (33), we see that the Lagrange multipliers μ_A and μ_B stand for the values of the bending moment at point A and B. In contrast to the curvature, the bending moment is found to be continuous at these points:

$$\mu_A = M_{1A} = \mathring{M}_A, \qquad \mu_B = M_{2B} = \mathring{M}_B. \tag{49}$$

By setting $\overline{\ell} = 0$, that is constraining the length ℓ of the overlapping region to a fixed value, the conventional problem of an elastica with a piecewise-constant bending stiffness would be obtained. However, the frictionless sliding condition between the two flexible sub-rods implies that the overlapping region length ℓ is free to vary. The first variation $\overline{\mathcal{L}}$ must therefore vanish for every variation $\overline{\ell} \neq 0$, and taking into account Eqs. (47), (48) we arrive at

$$\frac{a_1}{2} \left(\theta_{1A}'\right)^2 - \frac{a_1 + a_2}{2} \left(\mathring{\theta}_A'\right)^2 + \frac{a_2}{2} \left(\theta_{2C}'\right)^2 + \boldsymbol{R} \cdot \boldsymbol{t}_{2C} = 0. \tag{50}$$

For each of the three regions, we introduce the corresponding Hamiltonian (see Eq. (24))

$$\begin{aligned}
\mathcal{H}_1 &= \frac{a_1}{2} \left(\theta_1'(s)\right)^2 + N_{1t}(s), && s \in [0, L - \ell], \\
\mathring{\mathcal{H}} &= \frac{a_1 + a_2}{2} \left(\mathring{\theta}'(s)\right)^2 + \mathring{N}_t(s), && s \in [L - \ell, L], \\
\mathcal{H}_2 &= \frac{a_2}{2} \left(\theta_2'(s)\right)^2 + N_{2t}(s), && s \in [L, 2L - \ell],
\end{aligned} \tag{51}$$

where

$$N_{1t}(s) = \boldsymbol{R} \cdot \boldsymbol{t}_1(s), \qquad \mathring{N}_t(s) = \boldsymbol{R} \cdot \mathring{\boldsymbol{t}}(s), \qquad N_{2t}(s) = \boldsymbol{R} \cdot \boldsymbol{t}_2(s). \tag{52}$$

As no distributed loads are applied, each of these quantities is conserved in each region, $\mathcal{H}_1' = 0$, $\mathring{\mathcal{H}}' = 0$, and $\mathcal{H}_2' = 0$. Recalling the tangent vector continuity at point A, Eq. (39)$_1$, the *frictionless sliding condition* (50) is rewritten as

$$\mathcal{H}_1 + \mathcal{H}_2 = \mathring{\mathcal{H}}. \tag{53}$$

The set of three nonlinear ordinary differential equations (44), complemented by the boundary conditions (46), the frictionless sliding condition (53), and the interface conditions (48) form a well-defined boundary value problem (BVP) once the parameters a_1, a_2, L, ℓ_0 and loads T_l and T_r are set. Solving this nonlinear BVP leads to the, possibly non-unique, equilibrium configuration of the flexible sleeve system described by the inclinations $\theta_1(s)$, $\mathring{\theta}(s)$, and $\theta_2(s)$, and the overlapping length ℓ. It is worth highlighting that, in analogy with the elastica sling problem (Cazzolli and Dal Corso, 2024), by imposing the frictionless sliding condition (53), the specific compound rod is identified within the family of equilibrated compound systems of length $2L - \ell$ as the one providing a stationary value in ℓ for the corresponding potential $\mathcal{V}(\ell)$.

5. Interaction forces between the two sub-rods and corresponding internal forces

The equations governing the equilibrium have been obtained in the previous Section for the compound system, without providing any information about the interactions between the two sub-rods in the overlapping region. This aspect is addressed here with the aim to compute the values of the internal force $\mathring{\boldsymbol{N}}_j(s)$ and moment $\mathring{M}_j(s)$ present in the jth sub-rod ($j = 1, 2$). At equilibrium, the resultants of these forces and moments represent the global force and moment of the compound system:

$$\mathring{\boldsymbol{N}}(s) = \mathring{\boldsymbol{N}}_1(s) + \mathring{\boldsymbol{N}}_2(s) = \boldsymbol{R}, \qquad \mathring{M}(s) = \mathring{M}_1(s) + \mathring{M}_2(s). \tag{54}$$

The distribution rule for the moment $\mathring{M}_j(s)$ in the jth sub-rod easily follows from the linear constitutive bending relation (20) and Eq. (33)$_2$,

$$\mathring{M}_j(s) = \frac{a_j}{a_1 + a_2} \mathring{M}(s), \qquad j = 1, 2, \tag{55}$$

implying that the two internal moments are proportional one to each other through the bending stiffness ratio a_2/a_1

$$\frac{\mathring{M}_2(s)}{\mathring{M}_1(s)} = \frac{a_2}{a_1}. \tag{56}$$

In contrast with the internal moment $\mathring{M}_j(s)$, the evaluation of the internal force $\mathring{\boldsymbol{N}}_j(s)$ ($j = 1, 2$) requires a deeper analysis, developed in the next Subsections (and complemented by the Appendices).

5.1. Interaction at the end points of the overlapping region

In this Subsection, we will extend the micromechanical approaches introduced by Balabukh et al. (1970), Bigoni et al. (2015), Dal Corso et al. (2017), where a flexible rod was inserted into a flat or curved rigid channel with a clearance. It will be shown in Section 5.1.1 that the tangential component of the interaction force at transition point A is given by

$$\mathring{N}_{2At} = -\underbrace{\frac{a_2(2a_1 + a_2)}{(a_1 + a_2)^2}}_{\in(0,1)} \frac{M_A^2}{2a_1} = -\underbrace{\frac{a_2(2a_1 + a_2)}{(a_1 + a_2)^2}}_{\in(0,1)} \frac{a_1 \left(\theta_{1A}'\right)^2}{2} = -\frac{a_2(2a_1 + a_2)}{2a_1} \left(\mathring{\theta}_A'\right)^2, \tag{57}$$

and at point B given by

$$\mathring{N}_{1Bt} = -\underbrace{\frac{a_1(a_1 + 2a_2)}{(a_1 + a_2)^2}}_{\in(0,1)} \frac{M_B^2}{2a_2} = -\underbrace{\frac{a_1(a_1 + 2a_2)}{(a_1 + a_2)^2}}_{\in(0,1)} \frac{a_2 \left(\theta_{2B}'\right)^2}{2} = -\frac{a_1(a_1 + 2a_2)}{2a_2} \left(\mathring{\theta}_B'\right)^2, \tag{58}$$

showing that the axial force jump at the entrance of a flexible sleeve is always *smaller* in magnitude than that of the rigid limit studied in (Bigoni et al., 2015). On the other hand, the axial force jump vanishes for vanishing bending stiffness of the rod ending at the transition point. Furthermore, the obtained expressions imply that the Hamiltonian invariant $\mathcal{H}_j$ along the jth rod ($j = 1, 2$) is continuous at the corresponding transition point, and takes a negative value, see Section 5.1.2. The invariant $\mathcal{H}_j$ is expressed as a function of the sub-rods bending stiffnesses and the curvature at the transition point, namely

$$\mathring{\mathcal{H}}_{1A} = \mathcal{H}_1 = -\frac{a_1(a_1 + a_2)}{2a_2} \left(\mathring{\theta}_B'\right)^2 \leq 0, \qquad \mathring{\mathcal{H}}_{2B} = \mathcal{H}_2 = -\frac{a_2(a_1 + a_2)}{2a_1} \left(\mathring{\theta}_A'\right)^2 \leq 0. \tag{59}$$

Anticipating the absence of any distributed tangential force and interaction moment, a consequence of Eq. (59) is that *the equilibrium of the flexible sliding sleeve implies that each sub-rod is never subject to a tensile state*:

$$\left\{N_{1t}(s), \mathring{N}_{1t}(s), \mathring{N}_{2t}(s), N_{2t}(s)\right\} \leq 0, \qquad \forall s. \tag{60}$$

Additionally, force balance for sub-rod 1 at point A yields $\mathring{N}_{1At} - N_{1At} + \mathring{N}_{2At} = 0$ and Eq. (57) implies $\mathring{N}_{1At} > N_{1At}$. Consequently, the compression in sub-rod 1 is larger just outside the overlapping region (just before A) than inside it (just after A). As the same can be said for sub-rod 2 at point B, in summary we have

$$N_{1t}(L-\ell) < \left\{\mathring{N}_{1t}(L-\ell), \mathring{N}_{2t}(L-\ell)\right\} < 0, \qquad N_{2t}(L) < \left\{\mathring{N}_{1t}(L), \mathring{N}_{2t}(L)\right\} < 0. \tag{61}$$

Moreover, the ratio of the two invariants follows from Eq. (59) as

$$\frac{\mathcal{H}_1}{\mathcal{H}_2} = \left(\frac{a_1}{a_2}\frac{\mathring{M}_B}{\mathring{M}_A}\right)^2 = \left(\frac{\mathring{M}_{1B}}{\mathring{M}_{2A}}\right)^2 = \left(\frac{\theta'_{2B}}{\theta'_{1A}}\right)^2. \tag{62}$$

It is noted that, as found for the elastica sling problem (Cazzolli and Dal Corso, 2024), in the limit case of one sub-rod infinitely stiffer than the other, and in the case where the stiffer rod goes flat, the invariant associated with the softer sub-rod vanishes,

$$\text{if } \frac{a_j}{a_i} \to \infty \;\Rightarrow\; \mathcal{H}_i = 0, \qquad i,j = 1,2, \qquad i \neq j. \tag{63}$$

5.1.1. Interaction tangential forces from micromechanical approach

At each end point of the overlapping region, in the case the flexible sleeve has a clearance, two points can be identified: (i) the last cross-section having both sub-rods present and (ii) the last cross-section having both sub-rods with the same curvature. A sketch of the corresponding configuration is reported in Fig. 5 (left) for the left end point of the overlapping region, where the two points are called A^- and A^+. At these two points, the inclinations are noted θ^-_{1A} and $\mathring{\theta}^+_A$, and frictionless contact forces

$$\boldsymbol{F}^-_{A[12]} = -\boldsymbol{F}^-_{A[21]}, \qquad \boldsymbol{F}^+_{A[12]} = -\boldsymbol{F}^+_{A[21]} \tag{64}$$

are defined in such a way that $\boldsymbol{F}^{\pm}_{A[ij]}$ is the concentrated frictionless contact force exerted by the ith sub-rod on the jth sub-rod at point $A^{\pm}$ ($i,j = 1,2$ with $i \neq j$). It is observed that the contact forces at the two points are not self-balanced, therefore a non-null resultant $\boldsymbol{F}_{A[12]}$ is realized at the considered transition point A,

$$\boldsymbol{F}_{A[12]} = \boldsymbol{F}^+_{A[12]} + \boldsymbol{F}^-_{A[12]}. \tag{65}$$

As the following analysis is of interest under the assumption of small clearance, the distance between the points A^- and A^+ is approximated with the curvilinear distance d, and geometrically linear computations are performed.

The axial force $\mathring{N}^+_{2At}$ can be obtained from equilibrium as the projection of the contact force $\boldsymbol{F}^-_{A[12]}$ as follows (Fig. 5, center)

$$\mathring{N}^+_{2At} = -\left|\boldsymbol{F}^-_{A[12]}\right| \left|\mathring{\theta}^+_A - \theta^-_{1A}\right|, \tag{66}$$

while the bending moment $\mathring{M}^+_{2A}$ balances the moment realized by the contact force $\boldsymbol{F}^-_{A[12]}$ at the distance d (Fig. 5, center):

$$\left|\mathring{M}^+_{2A}\right| = a_2 \left|\mathring{\theta}^{+\prime}_A\right| = \left|\boldsymbol{F}^-_{A[12]}\right| d. \tag{67}$$

For the present analysis, we make use of the geometrically linear assumption, which is reasonable because the size of the zone we consider is small, and the local deformations are thus small as well. That means the results are also applicable in the general finite rotations but small strain setting, the inclination difference $\left|\mathring{\theta}^+_A - \theta^-_{1A}\right|$ for a rod of length d and stiffness a_1 is obtained through the superposition of the effects due to the moment $M^-_{1A} = a_1\theta^-_{1A}{}'$ and to the transverse concentrated force $\boldsymbol{F}^-_{A[21]}$ (Fig. 5, right),

$$\left|\mathring{\theta}^+_A - \theta^-_{1A}\right| = \left|\theta^-_{1A}{}'\right| d - \frac{\left|\boldsymbol{F}^-_{A[21]}\right| d^2}{2a_1}. \tag{68}$$

As the clearance vanishes, the distance d correspondingly approaches zero ($d \to 0$)[3] and the following limits hold

$$\mathring{N}^+_{2At} \to \mathring{N}_{2At}, \qquad \theta^-_{1A}{}' \to \theta'_{1A}, \qquad \mathring{\theta}^{+\prime}_A \to \mathring{\theta}'_A, \tag{69}$$

and using Eqs. (67), (68), (66), and $\left|\boldsymbol{F}^-_{A[12]}\right| = \left|\boldsymbol{F}^-_{A[21]}\right|$, the value of $\mathring{N}_{2At}$ is found to be given by Eq. (57). The negative sign in Eq. (57) implies that the end of sub-rod 2, in the overlapping region, is always subject to compression

$$\mathring{N}_{2At} \leq 0, \tag{70}$$

A similar result was found by Cazzolli and Dal Corso (2024) in the case of the elastica sling. Analogous computations at point B provide the value of $\mathring{N}_{1Bt}$, see Eq. (58), and also show that its end is under compression.

[3] It is worth mentioning that, differently from previous micromechanical calculations performed for a rigid sliding sleeve (Bigoni et al., 2015), the present passages show that the relation between the distance d and the clearance is unnecessary. Indeed, it is sufficient to consider the limit of vanishing distance $d \to 0$ to obtain the limiting value of the tangential resultant $\mathring{N}_{2At}$ provided by the two concentrated forces in the case of a perfect (zero-clearance), flexible, frictionless sliding sleeve.

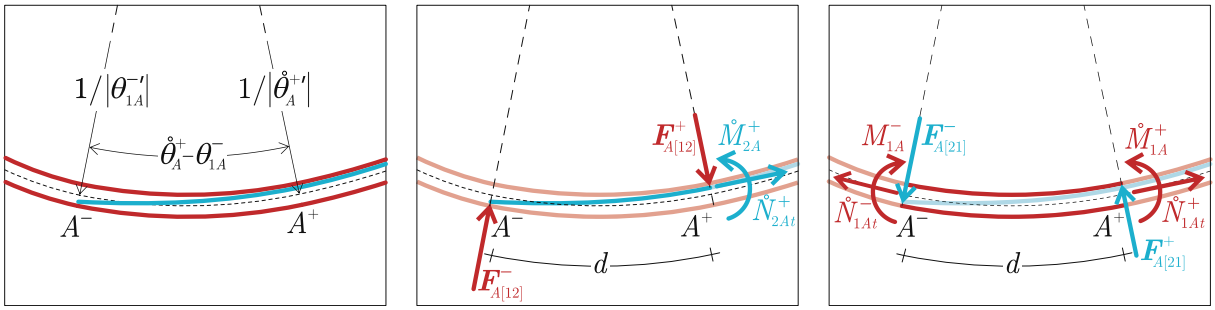

Fig. 5. Micromechanics at the left transition point (A) of a frictionless flexible sleeve, considered in the imperfect case of a small clearance. Deformed configuration showing contact points A^- and A^+ and the corresponding values of the radius of curvature ($1/\left|\theta_{1A}^{-\prime}\right|$ and $1/\left|\mathring{\theta}_A^{+\prime}\right|$), as well as the inclination difference $\left|\mathring{\theta}_A^{+}-\theta_{1A}^{-}\right|$ (left). Free-body diagram for sub-rod 2 (center) and sub-rod 1 (right).

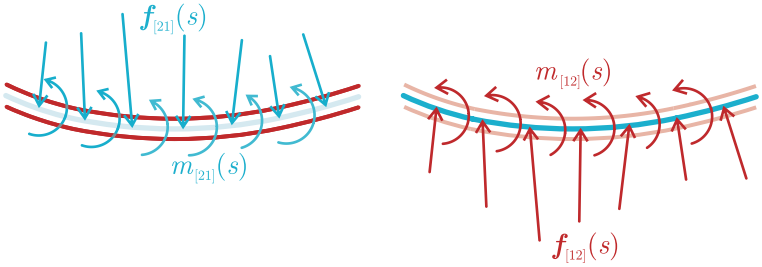

Fig. 6. Distributed interaction force $\boldsymbol{f}_{[ij]}(s)$ and moment $m_{[ij]}(s)$ exerted by the ith sub-rod on the jth sub-rod ($i,j=1,2$, with $j\neq i$) along the overlapping region $s\in(L-\ell,L)$ (the rods are drawn with an offset for the sake of visualization). Due to equilibrium, the two distributions satisfy Eq. (74). In Appendix B it is shown that, in the limit of unshearable and inextensible rods, the frictionless condition implies vanishing interaction moment and tangential interaction force, $m_{[ij]}(s)=f_{[ij]t}(s)=0$.

5.1.2. *Continuity of the invariant $\mathcal{H}$ along the same sub-rod at the transition point*

By considering the interface condition $(48)_1$ and expressing the curvature jump at point A, we rewrite the axial force $\mathring{N}_{2At}$ (57) as

$$\mathring{N}_{2At}=\frac{a_1}{2}\left[\left(\mathring{\theta}_A'\right)^2-\left(\theta_{1A}'\right)^2\right]\leq 0. \tag{71}$$

Furthermore, writing equilibrium relation $(54)_1$ at point A along the tangent direction yields

$$\mathring{N}_{2At}=N_{1At}-\mathring{N}_{1At}. \tag{72}$$

Then, by recalling the values $\mathcal{H}_1$ and $\mathring{\mathcal{H}}_{1A}$ of the Hamiltonian in sub-rod 1, respectively along its non-overlapping portion and at the end point of the overlapping region,

$$\mathcal{H}_1=N_{1At}+\frac{a_1}{2}\left(\theta_{1A}'\right)^2,\qquad \mathring{\mathcal{H}}_{1A}=\mathring{N}_{1At}+\frac{a_1}{2}\left(\mathring{\theta}_A'\right)^2, \tag{73}$$

it is seen that the Hamiltonian $\mathcal{H}$ along sub-rod 1 is continuous at the transition point A, Eq. $(59)_1$. An analogous calculation performed for sub-rod 2 at point B yields Eq. $(59)_2$. It follows that at point A (B) the interaction forces $\mathring{M}_{2A}^{+}$ and $\boldsymbol{F}_{A[21]}$ ($\mathring{M}_{1B}^{-}$ and $\boldsymbol{F}_{B[12]}$) satisfy the condition provided by Eq. (30).

It is finally noted that the continuity property (59) for the Hamiltonian can be alternatively obtained through the variational approach performed in the inextensible limit of extensible rods, as shown in Appendix B.1.

5.2. *Interaction along the overlapping region*

In addition to the concentrated forces at the transition points (investigated in the previous Subsection), the ith sub-rod exerts a distributed force $\boldsymbol{f}_{[ij]}(s)$ and a distributed moment $m_{[ij]}(s)$ on the jth sub-rod ($i,j=1,2$, with $j\neq i$), Fig. 6, which for equilibrium satisfy

$$\boldsymbol{f}_{[12]}(s)=-\boldsymbol{f}_{[21]}(s),\qquad m_{[12]}(s)=-m_{[21]}(s),\qquad s\in(L-\ell,L). \tag{74}$$

Considering these interaction force and moment, the equilibrium equations (22) and (21) can be written for the jth sub-rod as

$$\begin{cases} \mathring{N}'_{jt}(s) = -f_{[ij]t}(s) + \mathring{\theta}'(s)\mathring{N}_{jn}(s), \\ \mathring{N}'_{jn}(s) = -f_{[ij]n}(s) - \mathring{\theta}'(s)\mathring{N}_{jt}(s), \\ a_j\mathring{\theta}''(s) + \mathring{N}_{jn}(s) + m_{[ij]}(s) = 0, \end{cases} \qquad s \in [L-\ell, L], \qquad i,j = 1,2, \qquad i \neq j. \tag{75}$$

Recalling that the compound model is connected to the sub-rods model through Eq. (54), the summation over $j = 1,2$ of Eq. (75) leads to the equilibrium equations for the compound rod in the overlapping region

$$\begin{cases} \mathring{N}'_t(s) = \mathring{\theta}'(s)\mathring{N}_n(s), \\ \mathring{N}'_n(s) = -\mathring{\theta}'(s)\mathring{N}_t(s), \\ (a_1+a_2)\mathring{\theta}''(s) + \mathring{N}_n(s) = 0, \end{cases} \qquad s \in [L-\ell, L], \tag{76}$$

which are coherent with equilibrium equations (19a) and (21) with $\boldsymbol{f}(s) = \boldsymbol{f}_{[12]}(s) + \boldsymbol{f}_{[21]}(s) = \boldsymbol{0}$ and $m(s) = m_{[12]}(s) + m_{[21]}(s) = 0$, as well as the moment equilibrium of the compound system, $(44)_2$, obtained using a variational approach.

How the internal force $\mathring{\boldsymbol{N}}(s)$ of the compound system is distributed among the two sub-rods as $\mathring{\boldsymbol{N}}_1(s)$ and $\mathring{\boldsymbol{N}}_2(s)$ can only be settled through further information about $\boldsymbol{f}_{[ij]}(s)$ and $m_{[ij]}(s)$.

Zero moment and tangential distributed interaction forces. Intuitively, the frictionless sliding between the two sub-rods seems to be associated with the absence of distributed tangential force $f_{[ij]t}(s) = \boldsymbol{f}_{[ij]}(s) \cdot \mathring{\boldsymbol{t}}(s)$ and distributed moment $m_{[ij]}(s)$,

$$f_{[ij]t}(s) = m_{[ij]}(s) = 0, \quad s \in [L-\ell, L], \quad i,j = 1,2, \quad i \neq j. \tag{77}$$

We formally prove this absence in Appendices B.1 and B.2 through a variational approach involving axial and shear deformability of both sub-rods and their inextensible and unshearable limit.

Internal forces and Hamiltonian invariance for the overlapping sub-rods. In the light of Eq. (77), the equilibrium equations (75) imply the following distribution rule of the internal shear force $\mathring{N}_{jn}(s)$ in the jth sub-rod:

$$\mathring{N}_{jn}(s) = \frac{a_j}{a_1+a_2}\,\mathring{N}_n(s), \qquad s \in [L-\ell, L], \qquad j = 1,2. \tag{78}$$

Similarly to the distribution rule for the bending moments in Eq. (55), the internal shear forces in the sub-rods are thus proportional to each other through the bending stiffness ratio

$$\frac{\mathring{N}_{2n}(s)}{\mathring{N}_{1n}(s)} = \frac{a_2}{a_1}, \qquad s \in [L-\ell, L]. \tag{79}$$

However, the equilibrium considerations, including the jump conditions in the transition points, do not allow for drawing a conclusion regarding the distribution of the axial force $\mathring{N}_t = \mathring{N}_{1t} + \mathring{N}_{2t}$ between the sub-rods. This static indeterminacy is resolved either by using the micromechanical approach as of Section 5.1.1 or by the extended variational procedure, presented in Fig. B.14. Indeed, due to the vanishing of the interaction tangential force and moment (77), the conservation law Eq. (26) holds for each sub-rod in the overlapping region, and therefore

$$\mathring{\mathcal{H}}_j(s) = \frac{a_j}{2}\left(\mathring{\theta}'(s)\right)^2 + \mathring{N}_{jt}(s) = \mathring{\mathcal{H}}_j, \qquad s \in [L-\ell, L], \qquad j = 1,2. \tag{80}$$

Together with Eq. (59) this implies that the *Hamiltonian along each sub-rod composing the frictionless sliding sleeve has a unique constant value in both the overlapping and the non-overlapping regions*,

$$\mathring{\mathcal{H}}_j = \mathcal{H}_j, \qquad j = 1,2. \tag{81}$$

The exploitation of this important and elegant result in Eq. (53) and the projection of Eq. (54) along $\mathring{\boldsymbol{t}}(s)$ lead to the evaluation of the internal axial forces $\mathring{N}_{jt}(s)$ as

$$\left.\begin{matrix} \mathring{N}_{1t}(s) \\ \mathring{N}_{2t}(s) \end{matrix}\right\} = \frac{\mathring{N}_t(s)}{2} \pm \frac{1}{2}\left[\frac{a_2-a_1}{2}\left(\mathring{\theta}'(s)\right)^2 + \mathring{\mathcal{H}}_1 - \mathring{\mathcal{H}}_2\right], \qquad s \in [L-\ell, L]. \tag{82}$$

Furthermore, using Eqs. (51), (57), (58), and (81) we find that

$$\mathring{\mathcal{H}}_1 - \mathring{\mathcal{H}}_2 = \frac{a_1\,a_2}{2(a_1+a_2)}\left[\left(\theta'_{1A}\right)^2 - \left(\theta'_{2B}\right)^2\right]. \tag{83}$$

It follows that, unlike the shear forces $\mathring{N}_{jn}(s)$ and moment $\mathring{M}_j(s)$, Eqs. (56) and (79), the ratio of the internal axial forces $\mathring{N}_{jt}(s)$ is in general not constant:

$$\frac{\mathring{N}_{2t}(s)}{\mathring{N}_{1t}(s)} = \frac{a_2}{a_1}\,\frac{\mathring{N}_t(s) - \frac{a_1}{a_2}\left(\frac{a_2}{a_1}\mathring{\mathcal{H}}_1 - \mathring{\mathcal{H}}_2\right)}{\mathring{N}_t(s) + \frac{a_2}{a_1}\mathring{\mathcal{H}}_1 - \mathring{\mathcal{H}}_2}, \qquad s \in [L-\ell, L]. \tag{84}$$

Finally, from Eqs. (78) and (82), the internal force $\mathring{\boldsymbol{N}}_j(s)$ can be written as

$$\begin{aligned}\mathring{\boldsymbol{N}}_1(s) &= \frac{a_1}{a_1+a_2}\left[\boldsymbol{R} + \left(\frac{a_2}{a_1}\mathring{\mathcal{H}}_1 - \mathring{\mathcal{H}}_2\right)\mathring{\boldsymbol{t}}(s)\right],\\ \mathring{\boldsymbol{N}}_2(s) &= \frac{a_2}{a_1+a_2}\left[\boldsymbol{R} - \left(\mathring{\mathcal{H}}_1 - \frac{a_1}{a_2}\mathring{\mathcal{H}}_2\right)\mathring{\boldsymbol{t}}(s)\right],\end{aligned} \qquad s\in[L-\ell, L]. \tag{85}$$

The evaluation of the internal forces $\mathring{\boldsymbol{N}}_1(s)$ and $\mathring{\boldsymbol{N}}_2(s)$ at the transition points A and B provide the values of the interaction contact forces $\boldsymbol{F}_{A[12]}$ and $\boldsymbol{F}_{B[12]}$ as

$$\boldsymbol{F}_{A[12]} = -\mathring{\boldsymbol{N}}_2(L-\ell), \qquad \boldsymbol{F}_{B[21]} = \mathring{\boldsymbol{N}}_1(L). \tag{86}$$

Distributed normal interaction force. Inserting Eq. (85) in the sub-rod equilibrium equations (75) and introducing the (distributed normal) contact force parameter Λ_{ij} as

$$\Lambda_{ij} = \frac{a_j\,\mathcal{H}_i - a_i\mathcal{H}_j}{a_1+a_2}, \tag{87}$$

the normal component $f_{[ij]n}(s)$ of the distributed interaction force is evaluated to be

$$f_{[ij]n}(s) = \Lambda_{ij}\,\mathring{\theta}'(s), \qquad s\in(L-\ell, L), \qquad i,j=1,2, \qquad i\neq j, \tag{88}$$

which is linear in the local value of the curvature $\mathring{\theta}'(s)$, but nonlinear in the global bending amplitude of the system.

Small rotation limit. Even in the geometrically linear setting, when the rotation field $\theta(s)$ is assumed to have an amplitude scaling with a small parameter p, the invariant $\mathcal{H}$ is quadratic in the rotation amplitude and the normal component $f_{[ij]n}(s)$ of the distributed interaction force is cubic in p

$$\theta(s)\sim p \quad \Rightarrow \quad \mathcal{H}\sim p^2 \quad \Rightarrow \quad f_{[ij]n}(s)\sim p^3, \tag{89}$$

and therefore its contribution can be neglected in small rotation analyses as performed in Section 2.

Vanishing distributed interaction force. It is noted that, in addition to the trivial configuration $\theta(s)=0$, the ratio in the internal axial forces $\mathring{N}_{2t}(s)/\mathring{N}_{1t}(s)$ becomes constant and $f_{[ij]n}(s)$ vanishes in the particular case where

$$a_2\mathring{\mathcal{H}}_1 = a_1\mathring{\mathcal{H}}_2 \quad \Leftrightarrow \quad \left(\frac{\mathring{M}_B}{\mathring{M}_A}\right)^2 = \frac{a_2}{a_1} \quad \Rightarrow \quad \frac{\mathring{N}_{2t}(s)}{\mathring{N}_{1t}(s)} = \frac{a_2}{a_1} \quad \text{and} \quad f_{[ij]n}(s)=\Lambda_{ij}=0, \qquad s\in[L-\ell, L]. \tag{90}$$

This particular condition not only occurs under symmetric stiffness ($a_1=a_2$) and configuration ($\theta(s)=\theta(2L-s)$), but it may also occur under nonsymmetric conditions, as shown in the case study presented in Section 6.

Reconnecting with global equilibrium. It is finally remarked that by integrating Eq. (17)

$$\int_{L-\ell}^{L}\theta'(s)\,\boldsymbol{n}(s)\mathrm{d}s = \boldsymbol{t}(L) - \boldsymbol{t}(L-\ell), \tag{91}$$

and using Eqs. (85), (86), (88) the equilibrium of each sub-rod is automatically satisfied

$$\begin{aligned}-\boldsymbol{R} + \boldsymbol{F}_{A[21]} + \boldsymbol{F}_{B[21]} + \int_{L-\ell}^{L} f_{[21]n}\boldsymbol{n}(s)\mathrm{d}s = \boldsymbol{0}, \quad &\text{for sub-rod 1},\\ \boldsymbol{R} + \boldsymbol{F}_{A[12]} + \boldsymbol{F}_{B[12]} + \int_{L-\ell}^{L} f_{[12]n}\boldsymbol{n}(s)\mathrm{d}s = \boldsymbol{0}, \quad &\text{for sub-rod 2}.\end{aligned} \tag{92}$$

Moreover, the projection along $\boldsymbol{e}_x$ and $\boldsymbol{e}_y$ of Eq. (92) provides the reaction components R_x and R_y as

$$\begin{aligned}R_x &= \underbrace{\mathring{N}_{2At}\cos\theta_A - \mathring{N}_{2An}\sin\theta_A}_{-F_{A[12]x}} + \underbrace{\mathring{N}_{1Bt}\cos\theta_B - \mathring{N}_{1Bn}\sin\theta_B}_{-F_{B[12]x}} - \int_{L-\ell}^{L} f_{[12]n}(s)\sin\mathring{\theta}(s)\mathrm{d}s,\\ R_y &= \underbrace{\mathring{N}_{2At}\sin\theta_A + \mathring{N}_{2An}\cos\theta_A}_{-F_{A[12]y}} + \underbrace{\mathring{N}_{1Bt}\sin\theta_B + \mathring{N}_{1Bn}\cos\theta_B}_{-F_{B[12]y}} - \int_{L-\ell}^{L} f_{[12]n}(s)\cos\mathring{\theta}(s)\mathrm{d}s,\end{aligned} \tag{93}$$

whose approximated expressions under linearized kinematics were given by Eq. (13).

6. Results from nonlinear analysis and two different ejection mechanisms

6.1. Numerical solver for the nonlinear boundary value problem

We begin this Section with a brief presentation on our implementation of the shooting method for solving the nonlinear BVP governing the equilibrium of the compound rod model. The system features a set of three nonlinear differential (elastica)

```
In[1]:= zero[{ϑ0_?NumberQ, Nx_?NumberQ, Ny_?NumberQ, ℓ_?NumberQ}] := (
          sol = NDSolve[
              {(* balance *)M'[s] - Nx Sin[ϑ[s]] + Ny Cos[ϑ[s]] == 0,
               (* constitutive *)Piecewise[{{a1, s < L - ℓ}, {a1 + a2, s < L}}, a2] ϑ'[s] == M[s],
               (* kinematics *)x'[s] == Cos[ϑ[s]], y'[s] == Sin[ϑ[s]],
               (* initial values *)x[0] == 0, y[0] == 0, M[0] == -T0, ϑ[0] == ϑ0},
              {M, ϑ, x, y}, {s, 0, 2 L - ℓ}, MaxSteps → ∞, Method → "StiffnessSwitching"][[1]];
          (* invariants in the three segments *)
          {H1, H0, H2} = 1 / 2 * a ϑ'[s]^2 + Nx Cos[ϑ[s]] + Ny Sin[ϑ[s]] /. sol /.
            {{s → (L - ℓ) / 2, a → a1}, {s → L - ℓ / 2, a → a1 + a2}, {s → (3 L - ℓ) / 2, a → a2}};
          (* all conditions *){x[2 L - ℓ] - (2 L - ℓ0), y[2 L - ℓ] - 0, M[2 L - ℓ] + T0, H1 + H2 - H0} /. sol
         )

In[2]:= (* parameters of the model *)L = 1; a1 = 1.5; a2 = 1; ℓ0 = 0.5; T0 = 1;

In[3]:= (* solving the BVP *)goodValues = FindRoot[zero[{ϑ0, Nx, Ny, ℓ}], {ϑ0, 0.5}, {Nx, 0}, {Ny, 0}, {ℓ, ℓ0}]

Out[3]= {ϑ0 → 0.599768, Nx → -0.953121, Ny → 3.4774×10^-9, ℓ → 0.387902}

In[4]:= (* plotting the deformed shape *)
        Show[ParametricPlot[{x[s], y[s]} /. sol, {s, 0, 2 L - ℓ /. goodValues}],
         ParametricPlot[{x[s], y[s]} /. sol, {s, L, L - ℓ /. goodValues}, PlotStyle → Red], AxesLabel → {"x", "y"}]
```

Out[4]=

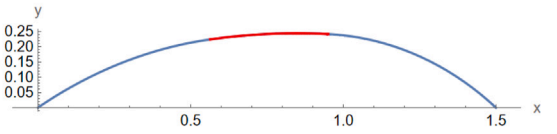

Fig. 7. Wolfram Mathematica source code for solving the nonlinear BVP using the method of shooting and computing the equilibrium configuration for symmetric external bending moments $T_r = T_l = T_0$. Out[4] provides the deformed configuration with the overlapping region displayed in red and the non-overlapping regions in blue.

equations (44), two boundary conditions (46), and the frictionless sliding condition (53) for the additional unknown ℓ. The Wolfram Mathematica[4] code featuring a minimal example for a nonsymmetric setup is demonstrated in Fig. 7. This code handles a case with symmetric loads $T_r = T_l = T_0$ but nonsymmetric rod properties $a_1 \neq a_2$, and it is easily extendable to other loading scenarios, as well as parametric studies.

The core of the implementation is the user function `zero`. Given a current guess of the rotation angle at the left support θ_0, the internal force components N_x and N_y (which are also the components of the reaction force $\boldsymbol{R}$ at the right support), and the overlapping length ℓ, this function solves an initial value problem using the routine `NDSolve`. This problem involves the equation for the equilibrium of moments, the constitutive relation defined piecewise as a function of the bending stiffness $a(s)$ (with Wolfram Mathematica correctly handling the jump conditions), and the kinematic relations for $x(s)$ and $y(s)$. As a result, the function returns the mismatches in the end positions $x(s_C)$, $y(s_C)$, the error in the end bending moment $M(s_C) + T_0$ as well as the residuum of the frictionless sliding condition $\mathcal{H}_1 + \mathcal{H}_2 - \mathring{\mathcal{H}}$. The `FindRoot` routine afterwards finds 'good values' of the guesses for θ_0, N_x, N_y and ℓ such that the residua vanish and all equilibrium equations are satisfied. The numerical values of the variables we solve for, as well as a plot of the deformed shape, are provided in the bottom of Fig. 7; the parameter set matches the values given in the caption of Fig. 4. It remains to mention that a non-material finite element model may alternatively be used for minimizing the total energy $\mathcal{V}$ as in Eq. (34) with respect to the configuration of the compound rod and the configurational parameter ℓ. For the details of the re-parametrization of the material coordinate s by a normalized one in each segment, such that the transition points always match with nodal points of the mesh, we refer to Vetyukov (2024) as well as to Vetyukov et al. (2024).

6.2. *First example: symmetric setup, ejection by snapping instability*

As a first example, we focus on a fully symmetric setup with $a_1 = a_2 = 1$, $L = 1$ and $\ell_0 = 0.5$ (SI system of units is used throughout the paper). The distributed interaction force Eq. (88) vanishes because of the symmetry of the setup $a_1 = a_2$ and of the solution $\mathcal{H}_1 = \mathcal{H}_2$, such that the sub-rods interact only at the transition points. Monotonically increasing the load factor $T_l = T_r = T_0$ in small steps from the unloaded state, we obtain an equilibrium path providing the overlapping length $\ell(T_0)$ and the mid-point deflection $y_{\text{mid}}(T_0)$ as plotted in Fig. 8. Note that the initial slope $\partial y_{\text{mid}}/\partial T_0\big|_{T_0=0}$ corresponds to the solution of the linear beam theory for unit moment load, while the horizontal tangent of the other curve with $\partial \ell/\partial T_0\big|_{T_0=0} = 0$ confirms that the overlapping length

[4] https://www.wolfram.com/mathematica

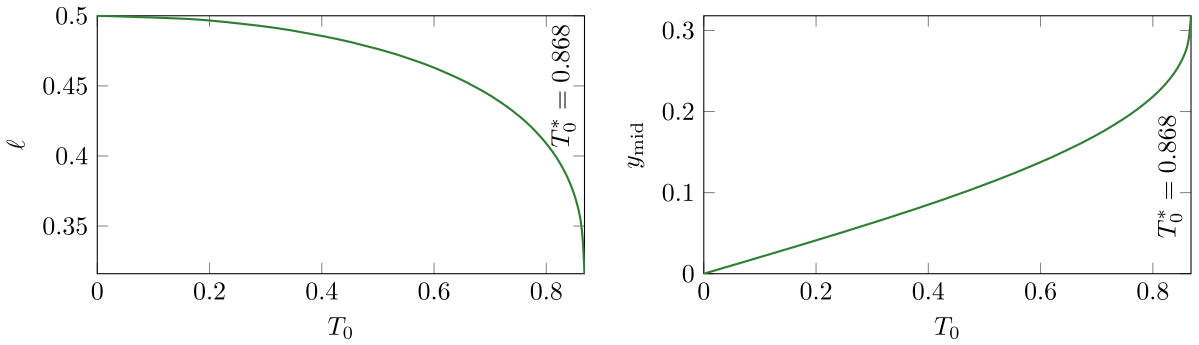

Fig. 8. Equilibrium path for the symmetric setup of Section 6.2, where $\ell_0 = 0.5$. The length of the overlapping region (left) and the maximum transverse deflection (right) are plotted as functions of the external moment T_0, showing both a vertical asymptote at the critical point T_0^*, with $\ell(T_0^*) \approx 0.32$.

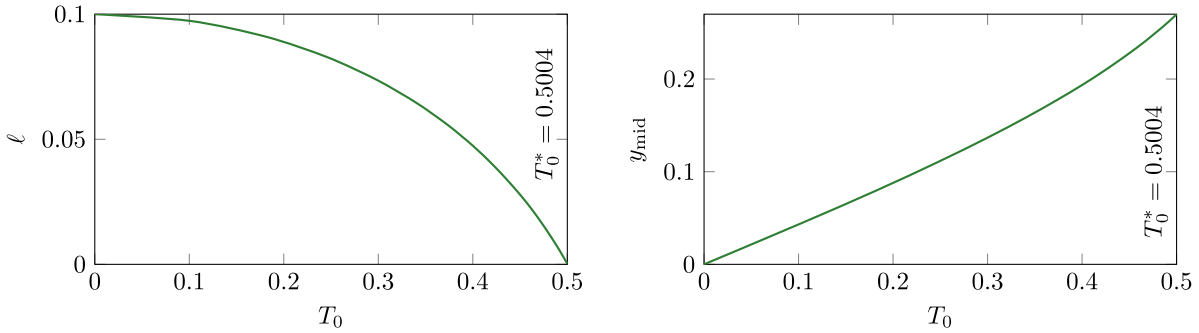

Fig. 9. Equilibrium path for the symmetric setup of Section 6.3, where $\ell_0 = 0.1$. The length of the overlapping region (left) and the maximum transverse deflection (right) are plotted as functions of the external moment T_0. Note that the length of the overlapping region vanishes at the critical point T_0^*.

change is a second order effect under small rotation conditions. As the moment loading progresses, the length ℓ decreases faster, while the deflection y_{mid} shows a softening behavior. Eventually, both curves approach a vertical asymptote at the critical moment value of $T_0^* = 0.868$, which represents the maximum bearing capacity and, for this system, is associated with a fold bifurcation of the equilibrium path and a snap-through instability. Although only a dynamic analysis could accurately describe this instability, it is expected that the two sub-rods will dynamically slip out from each other, starting from the length $\ell(T_0^*) \approx 0.32$ until complete expulsion. The hypothesis that full ejection results from the snapping instability is supported by the rapidly decreasing value of $\ell(T_0)$ beforce the snapping point. We also remark that no equilibria with overlapping regions could be found in numerical experiments for $T_0 > T_0^*$.

The catastrophic scenario of complete expulsion can be explained in simple words by the self-destabilizing property of the horizontal reaction force R_x. Indeed, this repelling force is growing proportional to the square of the curvature. When the deflections $y(s)$ become substantial, this constraint reaction begins to contribute to the bending moment and thus to the curvature. This positive feedback results in a stability loss.

6.3. Second example: symmetric setup, ejection by exhausting the overlapping length

This second example differs from the first one just in the value of ℓ_0: the initial length of the overlapping region $\ell = 0.1$ is now small. From the respective simulation results plotted for $\ell(T_0)$, $y_{\text{mid}}(T_0)$ in Fig. 9, we observe that the maximum bearing capacity is reached now without any stiffness loss, but is associated with a different scenario: the vanishing of the overlapping length ℓ at the critical moment value $T_0^* = 0.5004$. A limited softening can be also seen in the deflection behavior at growing load. Interestingly, an attempt to estimate the critical moment value T_0^* by simple geometrical considerations fails: assuming the rod to have a constant curvature given by $T_0^*/a_1 \approx 0.5$ in the critical state $\ell = 0$ and knowing its total length $2L = 2$, we would compute the distance between the end points of this circular arc as $4\sin(0.5) = 1.9177 > 1.9$. This means that the curvature must be significantly higher and underlines the importance of the compressive force in the elastic response. An accurate analytical estimation of T_0^* using the second order beam theory is possible, although non-trivial.

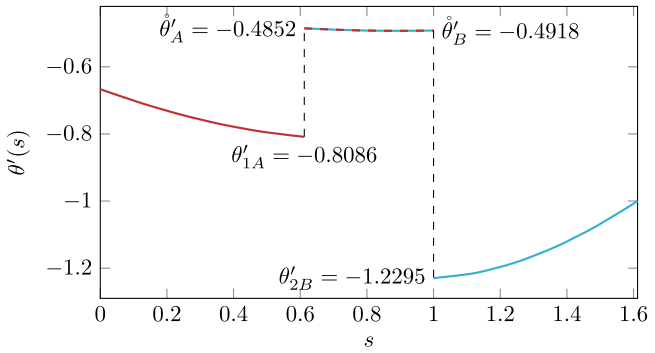

Fig. 10. Curvature distribution for the unsymmetric setup of Section 6.4, where $a_1 = 1.5 \neq a_2 = 1$.

6.4. Third example: nonsymmetric case, analysis of axial force

We now consider symmetric external loads $T_r = T_l = T_0 = 1$ but unequal bending rigidities $a_1 = 1.5$, $a_2 = 1$, while $L = 1$ and $\ell_0 = 0.5$. This corresponds to the (nonsymmetrical) configuration shown in Fig. 4, which is computed in Fig. 7, and results in[5]

$$\ell = 0.3879, \quad N_x = -0.9532, \quad N_y = 0, \quad \mathcal{H}_1 = -0.4535, \quad \mathring{\mathcal{H}} = -0.6497, \quad \mathcal{H}_2 = -0.1962, \tag{94}$$

confirming that the sliding condition Eq. (53) is satisfied. In Fig. 10 we plot the curvature $\theta'(s)$ and specify respective values at the transition points. These values naturally satisfy the jump conditions, Eq. (48). Moreover, the square of the ratio of the curvatures at the transition points equals the ratio of the Hamiltonian invariants, as stated by Eq. (62).

Distribution of the axial force N_t in the entire compound rod and in the individual sub-rods is shown in Fig. 11. While in the left and right segments we merely plot $N_{it} = N_t = -\boldsymbol{R}\cdot\boldsymbol{t} = R_x\cos\theta$ (because $R_y = 0$), in the overlapping region we make use of the continuity of the invariants Eq. (81) and evaluate the tension in the sub-rods according to Eq. (73) as $N_{it} = \mathcal{H}_i - a_i(\mathring{\theta}')^2/2$. Plotting the distributions using Eq. (82), we would of course obtain identical curves. In Fig. 11 we also indicate the jumps in the axial forces within the sub-rods, which are the tangential components of the interaction forces acting between the sub-rods at the transition points. The magnitudes of these jumps perfectly correspond to the results of computations using Eq. (71) with the curvatures as in Fig. 10.

We conclude the example by demonstrating the balance of forces for the sub-rod 2 according to Eq. (92). From the solution of the BVP, we obtain the rotation angles at the two transition points, $\theta_A = 0.13979$ and $\theta_B = -0.050601$, which determines the respective unit tangent vectors $\mathring{\boldsymbol{t}}_A$ and $\mathring{\boldsymbol{t}}_B$. Using now Eqs. (85) and (86), we evaluate the concentrated interaction forces exerted by sub-rod 1 on sub-rod 2 at the transition points A and B:

$$\boldsymbol{F}_{A[12]} = 0.31822\,\boldsymbol{e}_x - 0.00887\,\boldsymbol{e}_y, \quad \boldsymbol{F}_{B[12]} = 0.63554\,\boldsymbol{e}_x - 0.00322\,\boldsymbol{e}_y. \tag{95}$$

We find the interaction force in the overlapping region by using Eq. (88) as

$$\boldsymbol{f}_{[12]}(s) = f_{[12]n}(s)\mathring{\boldsymbol{n}}(s) = \Lambda_{12}\,\mathring{\theta}'(s)\,\mathring{\boldsymbol{n}}(s), \tag{96}$$

where the numerical value of the contact force parameter is $\Lambda_{12} = -0.06369$. The integral of $\boldsymbol{f}_{[12]}$ over the overlapping region can be computed numerically using the numerical solution $\mathring{\theta}(s)$ of the BVP. The identity expressed by Eq. (91), however, allows to avoid the integration and the resultant of $\boldsymbol{f}_{[12]}$ can be evaluated as

$$\int_{L-\ell}^{L} \Lambda_{12}\,\mathring{\theta}'(s)\,\mathring{\boldsymbol{n}}(s)\,\mathrm{d}s = \Lambda_{12}\,(\boldsymbol{t}_B - \boldsymbol{t}_A) = -0.00054\,\boldsymbol{e}_x + 0.01210\,\boldsymbol{e}_y. \tag{97}$$

Adding the different terms according to Eq. (92) and taking into account $\boldsymbol{R} = N_x\boldsymbol{e}_x = -0.953217\,\boldsymbol{e}_x$, we obtain a zero vector up to a small round-off error. The computation also gives an indication on the orders of magnitude of different forces for the considered case: the horizontal interaction is dominant and is almost solely due to the concentrated forces, while the contribution of pressure $f_{[12]n}$ to the balance of forces in the x direction is of minor importance. Regarding the force balance in the y direction, all three terms are of the same order of magnitude.

[5] A Wolfram Mathematica notebook featuring computations, presented in this subsection is provided in Supplementary Material.

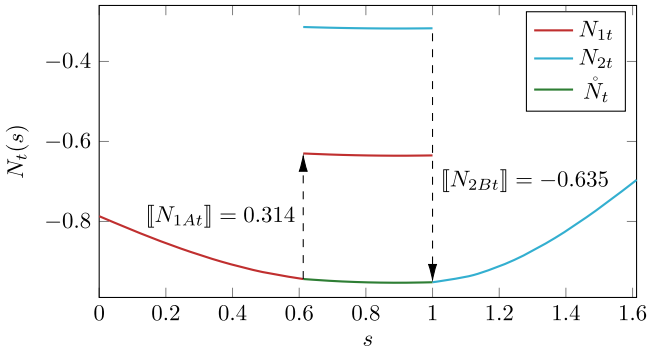

Fig. 11. Distribution of the tension (axial force) in the sub-rods for the unsymmetric setup of Section 6.4, where $a_1 = 1.5 \neq a_2 = 1$.

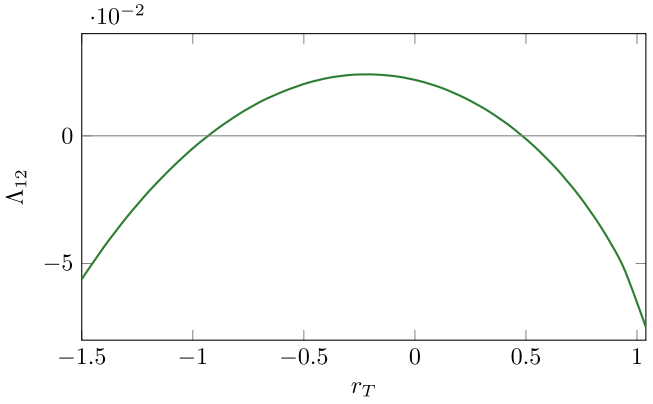

Fig. 12. Contact force parameter Λ_{12} (87) as a function of the moment ratio r_T for the nonsymmetric example of Section 6.5. Within the considered range, the plot shows that two different values exist for the moment ratio $r_T \approx \{-0.93, 0.48\}$ such that the contact force parameter vanishes, $\Lambda_{12} = 0$. For these two values the distributed normal contact force between the two sub-rods identically vanishes along the entire overlapping region.

6.5. Fourth example: changing sign of the distributed contact force in the overlapping region

In this last example, we consider the same setting as in the third one, but vary the bending moment at the right end according to the factor r_T:

$$T_l = 1, \quad T_r = r_T. \tag{98}$$

In doing so, we aim to demonstrate that the contact force parameter Λ_{12} in Eq. (96) (see also Eq. (88)) may vanish and change sign. The consequence is that there would be no normal distributed contact force, $f_{[12]n} = 0$, and therefore the sub-rods would interact only at the transition points even in an essentially nonsymmetric setup ($a_1 \neq a_2$ and $T_r \neq T_l$). The simulation results shown in Fig. 12 demonstrate that indeed the contact force parameter Λ_{12} turns out to vanish for at least one positive ($r_T \approx 0.48$) and one negative ($r_T \approx -0.93$) value of the moment ratio r_T ($r_T < 0$ corresponds to a loading in which the bending moments left and right are acting in the same direction, yielding a deformed state with an inflection point).

In Fig. 13 we demonstrate the deformed states and (differently scaled) distributions of the contact force in the overlapping region for three values of $r_T = \{-1.3, 0, 1\}$. We see the change in the direction of $f_{[12]n}$ between $r_T = 1$ (equal moments left and right) and $r_T = 0$ (no moment right), in agreement with the value $r_T \approx 0.48$ for which the distributed contact force vanishes. Additionally, we show that $f_{[12]n}(s)$ changes sign along the overlapping region when an inflection point $\hat{\theta}'(s) = 0$ is present, as in the case where $r_T = -1.3$.

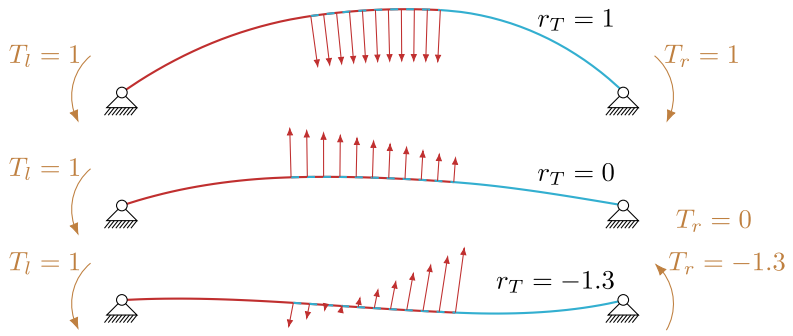

Fig. 13. Deformed shapes and distribution of normal contact force for different moment ratios $r_T = \{-1.3, 0, 1\}$, see Section 6.5. The normal force distribution changes direction when the moment is reduced at the right end, and the force vanishes at the inflection point when $r_T = -1.3$. Note that, for simplicity of representation, only the contact force distribution is plotted, while the concentrated interaction forces and moments at the transition points are not represented.

7. Conclusion

We have extended the analysis of planar flexible structures constrained by a frictionless sliding sleeve to the case where the constraint itself is also flexible, uncovering the equilibrium configuration and interaction between the two sub-rods. To achieve this, we first applied a variational approach to the compound system, deriving the equilibrium equations that govern its shape. These correspond to the well-known nonlinear differential equation of the elastica, adapted to reflect the bending stiffness of each relevant portion of the compound system, now complemented by a nonlinear algebraic equation interpreted as a frictionless sliding condition. The nonlinear algebraic equation ensures stationarity of the potential energy with respect to the overlapping length – measuring the interaction region where the two sub-rods remain in contact – at equilibrium. Furthermore, by employing both micromechanical and variational approaches to the system, modeled as two distinct sub-rods, we derive closed-form expressions for the interaction forces and moments. These expressions allow to describe both the concentrated and distributed interaction occurring respectively at the contact end points and across the whole contact region, revealing their dependence on the bending stiffnesses of the two sub-rods. More specifically, we demonstrated that, at equilibrium:

- whenever the flexible sleeve is bent, each sub-rod is entirely under compression (negative internal axial force, $N_t < 0$), meaning the interaction between the two sub-rods is of a '*repulsive*' nature (with magnitude bounded by the value of the rigid limit (Bigoni et al., 2015));
- the interaction within the overlapping region occurs solely through a normal contact force distribution f_n, while both tangential force and moment distributions are zero, $f_t = 0$ and $m = 0$. The local value of the normal distributed force is directly proportional to the local curvature, modulated by a multiplicative factor that may vanish under specific configurations, but yet depends nonlinearly on the global bending amplitude of the system;
- the Hamiltonian $\mathcal{H}_j$, defined as the sum of bending energy density and internal axial force, remains conserved along the j-th sub-rod. Consequently, it has no discontinuity at the end points of the contact region, despite the presence of concentrated interaction forces and moments.

It is noted that the continuity of $\mathcal{H}_j$ associated with the jth sub-rod at the respective transition point can be understood from the micromechanical approach, since the interaction forces there are normal to the relevant jth sub-rod and the Hamiltonian $\mathcal{H}_j$ is known to be conserved in the presence of normal (frictionless) contact forces (O'Reilly, 2017; Neukirch and Bertails-Descoubes, 2025) as evident from Fig. 5. Moreover, the present finding regarding the continuity of $\mathcal{H}_j$ at transition points is consistent with the observation that jumps of $\mathcal{H}_j$ are due to pseudomomentums or configurational forces (Hanna et al., 2018; O'Reilly, 2017).

Through the development of a simple numerical code, we analyzed various case studies, uncovering two distinct mechanisms of attaining the load-bearing capacity of the flexible sliding sleeve. Broadly speaking, our results suggest that the maximum capacity is attained either through a quasi-static, complete loss of overlap between the two sub-rods – occurring when the initial overlapping length of the flexible sleeve in its unloaded state is small – or through a snap-through instability when the initial overlapping length is larger. In the latter case, reaching the critical state is expected to trigger a dynamic sliding of the rods out of each other.

This study lays the foundation for a new framework in the mechanics of deployable structures, highlighting several promising directions for future development. These encompass frictional contact, spatial configurations, sub-rods with nonzero intrinsic curvatures, buckling analysis, multi-stability, and dynamic conditions.

CRediT authorship contribution statement

Sebastien Neukirch: Writing – review & editing, Writing – original draft, Validation, Methodology, Investigation, Formal analysis. **Francesco Dal Corso:** Writing – review & editing, Writing – original draft, Visualization, Validation, Methodology, Investigation, Formal analysis. **Yury Vetyukov:** Writing – review & editing, Writing – original draft, Visualization, Validation, Software, Methodology, Investigation, Formal analysis, Conceptualization.

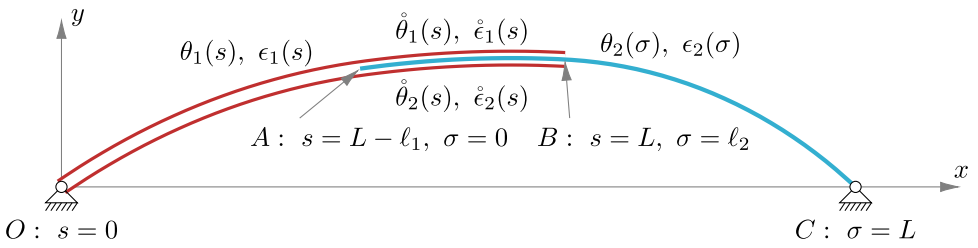

Fig. B.14. A configuration where both the inner rod and the flexible sleeve are extensible. The axial strains are noted $\epsilon_1(s)$ and $\epsilon_2(\sigma)$. In the overlapping region, the deformed length of both rods is the same, but their referential lengths ℓ_1 and ℓ_2 are different, see Eq. (B.4).

Declaration of competing interest

The authors declare the following financial interests/personal relationships which may be considered as potential competing interests: Francesco Dal Corso reports financial support was provided by European Research Council. If there are other authors, they declare that they have no known competing financial interests or personal relationships that could have appeared to influence the work reported in this paper.

Acknowledgments

SN acknowledges funding from the Horizon Europe Framework Programme (Grant agreement HORIZON-101205621), the french DIM MaTerRE (Grant INTIMAL), and the french IDEX Univ. of Paris (Grant Emergence DynaVine). FDC acknowledges funding from the European Research Council (ERC) under the European Union's Horizon Europe research and innovation programme, Grant agreement No. ERC-ADG-2021-101052956-BEYOND. The authors acknowledge TU Wien Bibliothek, Austria for financial support through its Open Access Funding Programme.

Appendix A. Complementary expressions for Section 2.2

The strain energy computed from the internal moment $M(s)$ reads

$$\mathcal{E}(\ell) = \frac{T_l^2}{2a_1a_2(a_1+a_2)}\left[a_2^2 Z(L-\ell,\ell) - a_1^2 Z(L,\ell) + a_1(a_1+a_2)Z(2L-\ell,\ell)\right], \tag{A.1}$$

with

$$Z(s,\ell) = s + \frac{R_y(\ell)}{T_l}s^2 + \left[\frac{R_y(\ell)}{T_l}\right]^2 \frac{s^3}{3}. \tag{A.2}$$

The dimensionless parameter ρ is then obtained as

$$\begin{aligned}\rho = \frac{1}{6r_a(1+r_a)(2-r_\ell)^3}\Big\{&r_a^2\left[10+10r_T+4r_T^2-3r_\ell(4+5r_T+3r_T^2)\right]\\ &+4+10r_T+10r_T^2-3r_\ell(3+5r_T+4r_T^2)+\left(1+r_T+r_T^2\right)\left[r_a(2-r_\ell)^3+r_\ell^2(6-r_\ell)(1+r_a^2)\right]\Big\},\end{aligned} \tag{A.3}$$

where

$$r_a = \frac{a_2}{a_1}, \qquad r_\ell = \frac{\ell}{L}, \qquad r_T = \frac{T_r}{T_l}. \tag{A.4}$$

Appendix B. Computing the internal axial and shear forces in each of the sub-rods along the overlapping region

In Section 4, we have derived equations for the equilibrium shape $(\mathring{x}, \mathring{y}, \mathring{\theta}, \mathring{\theta}')$ of the compound system (consisting of the two rods) in the overlapping region. In addition to this shape, we would like to have access to the internal forces $\mathring{\boldsymbol{N}}_1(s)$ and $\mathring{\boldsymbol{N}}_2(s)$ in each rod. In the overlapping region, the two rods are in interaction, potentially with both distributed contact forces and moments, that is the equilibrium for their internal forces and moments is given by system (75). Comparing $(44)_2$ with $(75)_3$ we see that due to the possible presence of moment interaction, we cannot yet infer the value of $\mathring{N}_{1n}(s)$ and $\mathring{N}_{2n}(s)$. Indeed (75) is a system of 6 scalar equations for 7 scalar unknowns $\mathring{N}_{1n}$, $\mathring{N}_{1t}$, $f_{[12]n}$, $f_{[12]t}$, $m_{[12]}$, $\mathring{N}_{2n}$, $\mathring{N}_{2t}$ and is hence underdetermined. Consequently, we set out to compute the internal axial force ($\mathring{N}_{1t}$ and $\mathring{N}_{2t}$) in each rod in order to reduce the number of unknowns to 5.

B.1. Inextensible limit of extensible sliding rods for deriving the internal axial forces $\mathring{N}_{1t}$ and $\mathring{N}_{2t}$

The variational problem treated in Section 4 for inextensible rods is enhanced to take into account a possible, although small, extensibility of the rod's and sleeve's axes. Assuming a linear constitutive relation in the axial response through the axial elastic stiffness b (sometimes called EA in Strength of Materials texts) and denoting the axial strain field with $\epsilon(s) > -1$, the axial force component $N_t(s)$ is given by

$$N_t(s) = b\,\epsilon(s). \tag{B.1}$$

Due to extensibility, the introduction of an additional curvilinear coordinate, $\sigma \in [0, L]$, is instrumental for describing the referential position along sub-rod 2, in addition to the curvilinear coordinate $s \in [0, L]$ describing the referential position along the sub-rod 1. It follows that by defining ℓ_1 and ℓ_2 as the referential overlapping length of each sub-rod, the interaction domains correspond to the subsets $s \in [L - \ell_1, L]$ and $\sigma = [0, \ell_2]$. Along these interaction domains, the deformed arclength is the same and hence the following identity holds for two infinitesimal elements in frictionless contact

$$[1 + \mathring{\epsilon}_2(\sigma)]\,\mathrm{d}\sigma = [1 + \mathring{\epsilon}_1(s)]\,\mathrm{d}s, \tag{B.2}$$

which is used to obtain the one-to-one integral relation between σ and s

$$\int_0^{\sigma} [1 + \mathring{\epsilon}_2(\sigma)]\,\mathrm{d}\sigma = \int_{L-\ell_1}^{s} [1 + \mathring{\epsilon}_1(s)]\,\mathrm{d}s, \tag{B.3}$$

implying that, although constrained to have the same deformed length, the two interaction domains have different referential lengths ℓ_1 and ℓ_2,

$$\ell_2 + \int_0^{\ell_2} \mathring{\epsilon}_2(\sigma)\,\mathrm{d}\sigma = \ell_1 + \int_{L-\ell_1}^{L} \mathring{\epsilon}_1(s)\,\mathrm{d}s. \tag{B.4}$$

It is also interesting to observe that, if a reparametrization on s is performed for the axial strain in the sub-rod 2, $\mathring{\epsilon}_2(s) \equiv \mathring{\epsilon}_2(\sigma)$, the one-to-one mapping of s into σ can be described as

$$\sigma\left(s, \mathring{\epsilon}_1, \mathring{\epsilon}_2\right) = \int_{L-\ell_1}^{s} \frac{1 + \mathring{\epsilon}_1(s)}{1 + \mathring{\epsilon}_2(s)}\,\mathrm{d}s. \tag{B.5}$$

The elastic energy $\mathcal{E}$ of the extensible and flexible sliding sleeve system can be evaluated as

$$\mathcal{E} = \mathcal{E}_1 + \mathring{\mathcal{E}}_1 + \mathring{\mathcal{E}}_2 + \mathcal{E}_2, \tag{B.6}$$

where the energy is split to consider the different contributions of the different sub-rods in the non-overlapping and overlapping regions

$$\mathcal{E}_1 = \frac{1}{2}\int_0^{L-\ell_1} \left[a_1\,\left(\theta_1'(s)\right)^2 + b_1\,\left(\epsilon_1(s)\right)^2\right]\mathrm{d}s, \tag{B.7a}$$

$$\mathring{\mathcal{E}}_1 = \frac{1}{2}\int_{L-\ell_1}^{L} \left[a_1\,\left(\mathring{\theta}_1'(s)\right)^2 + b_1\,\left(\mathring{\epsilon}_1(s)\right)^2\right]\mathrm{d}s, \tag{B.7b}$$

$$\mathring{\mathcal{E}}_2 = \frac{1}{2}\int_0^{\ell_2} \left[a_2\,\left(\mathring{\theta}_2'(\sigma)\right)^2 + b_2\,\left(\mathring{\epsilon}_2(\sigma)\right)^2\right]\mathrm{d}\sigma, \tag{B.7c}$$

$$\mathcal{E}_2 = \frac{1}{2}\int_{\ell_2}^{L} \left[a_2\,\left(\theta_2'(\sigma)\right)^2 + b_2\,\left(\epsilon_2(\sigma)\right)^2\right]\mathrm{d}\sigma, \tag{B.7d}$$

with the prime denoting differentiation with respect to the relevant space variable, s or σ.

The rotation $\{\theta_1(s), \mathring{\theta}_1(s), \mathring{\theta}_2(\sigma), \theta_2(\sigma)\}$ and the strain $\{\epsilon(s), \mathring{\epsilon}_1(s), \mathring{\epsilon}_2(\sigma), \epsilon_2(\sigma)\}$ fields are subject to the following constraints:

$$d_A = \theta_1(s = L - \ell_1) - \mathring{\theta}_1(s = L - \ell_1) = 0, \tag{B.8a}$$

$$d_B = \mathring{\theta}_2(\sigma = \ell_2) - \theta_2(\sigma = \ell_2) = 0, \tag{B.8b}$$

$$\boldsymbol{d}_C = \int_0^{L-\ell_1} (1 + \epsilon_1(s))\boldsymbol{t}_1(s)\,\mathrm{d}s + \int_{L-\ell_1}^{L} (1 + \mathring{\epsilon}_1(s))\mathring{\boldsymbol{t}}_1(s)\,\mathrm{d}s + \int_{\ell_2}^{L} (1 + \epsilon_2(\sigma))\boldsymbol{t}_2(\sigma)\,\mathrm{d}\sigma - (2L - \ell_0)\boldsymbol{e}_x = \boldsymbol{0}, \tag{B.8c}$$

$$d_e = \ell_2 - \ell_1 + \int_0^{\ell_2} \mathring{\epsilon}_2(\sigma)\,\mathrm{d}\sigma - \int_{L-\ell_1}^{L} \mathring{\epsilon}_1(s)\,\mathrm{d}s = 0, \tag{B.8d}$$

$$d_f(s) = \mathring{\theta}_1(s) - \mathring{\theta}_2\left(\sigma\left(s, \mathring{\epsilon}_1, \mathring{\epsilon}_2\right)\right) = 0, \qquad s \in [L - \ell_1, L]. \tag{B.8e}$$

Although the analytical derivation of the stationarity condition for the potential energy $\mathcal{V}$ can be addressed in the most general extensible case, for conciseness, this analysis is performed by considering only the leading order terms in the axial strain ($\epsilon \to 0$) as it is assumed that the axial strain energy density is much smaller than the bending energy density, namely

$$b\epsilon^2 \ll a\left(\theta'\right)^2.$$

Considering that the axial force component has the same magnitude as the bending moment divided by the rod's length,

$$b\,|\epsilon| \sim \frac{a\,|\theta'|}{L},$$

the following inequality holds for the bending and axial stiffnesses

$$\frac{bL^2}{a} \gg 1, \tag{B.9}$$

which in turn implies an inequality for the axial strain and the curvature

$$|\epsilon| \ll L\,|\theta'|\,. \tag{B.10}$$

Under the condition of small axial strains ($|\varepsilon| \sim |\epsilon| \ll 1$), Eq. (B.2) can be used to obtain the linearized expression of the undeformed infinitesimal length $\mathrm{d}\sigma$ as

$$\mathrm{d}\sigma = \left[1 + \mathring{\varepsilon}_1(s) - \mathring{\varepsilon}_2(s)\right]\,\mathrm{d}s, \qquad s \in [L-\ell_1, L], \tag{B.11}$$

and consequently Eq. (B.5) can be simplified to

$$\sigma\left(s, \mathring{\varepsilon}_1, \mathring{\varepsilon}_2\right) = s - (L-\ell_1) + \int_{L-\ell_1}^{s} \left[\mathring{\varepsilon}_1(s) - \mathring{\varepsilon}_2(s)\right]\,\mathrm{d}s, \qquad s \in [L-\ell_1, L], \tag{B.12}$$

which allows us to rewrite d_e as

$$d_e = \ell_2 - \ell_1 - \int_{L-\ell_1}^{L} \left[\mathring{\varepsilon}_1(s) - \mathring{\varepsilon}_2(s)\right]\,\mathrm{d}s = 0. \tag{B.13}$$

By further introducing the reparametrization $\mathring{\vartheta}_2(s) \equiv \mathring{\theta}_2(\sigma)$ and using the chain rule and Eq. (B.11), it is found

$$\mathring{\theta}_2'(\sigma) = \frac{\mathrm{d}}{\mathrm{d}\sigma}\mathring{\theta}_2(\sigma) = \frac{\mathrm{d}s}{\mathrm{d}\sigma}\frac{\mathrm{d}}{\mathrm{d}s}\mathring{\vartheta}_2(s) = \left[1 - \mathring{\varepsilon}_1(s) + \mathring{\varepsilon}_2(s)\right]\mathring{\vartheta}_2'(s). \tag{B.14}$$

Consequently, the energy $\mathring{\mathcal{E}}_2$ of sub-rod 2 in the overlapping region, Eq. (B.7c), can be rewritten as

$$\mathring{\mathcal{E}}_2 = \frac{1}{2}\int_{L-\ell_1}^{L} \left\{ a_2\,\left(\mathring{\vartheta}_2'(s)\right)^2\,\left[1 - \mathring{\varepsilon}_1(s) + \mathring{\varepsilon}_2(s)\right] + b_2\,\left(\mathring{\varepsilon}_2(s)\right)^2\,\left[1 + \mathring{\varepsilon}_1(s) - \mathring{\varepsilon}_2(s)\right] \right\}\,\mathrm{d}s, \tag{B.15}$$

and, since Eq. (B.8e) implies $\mathring{\theta}_1(s) = \mathring{\vartheta}_2(s)$ for $s \in [L-\ell_1, L]$, the elastic energy in the overlapping region can be simplified to

$$\mathring{\mathcal{E}}_1 + \mathring{\mathcal{E}}_2 = \frac{1}{2}\int_{L-\ell_1}^{L} \left\{ \left(\mathring{\theta}_1'(s)\right)^2\,[a_1 + a_2\,(1 - \mathring{\varepsilon}_1(s) + \mathring{\varepsilon}_2(s))] + b_1\,\left(\mathring{\varepsilon}_1(s)\right)^2 + b_2\,\left(\mathring{\varepsilon}_2(s)\right)^2 \right\}\,\mathrm{d}s, \tag{B.16}$$

where only the respective leading order terms in ϵ for the bending and axial energies are retained. With this new expression Eq. (B.16), the stationarity condition for $\mathcal{V} = \mathcal{E} - \mathcal{W}$ can be evaluated under the constraints (B.8a), (B.8c), (B.13), and with d_B rewritten as

$$d_B = \mathring{\theta}_1(s = L) - \theta_2(\sigma = \ell_2) = 0\,. \tag{B.17}$$

The stationarity of $\mathcal{V}$ is then performed by addressing the vanishing of the first variation of the Lagrangian $\mathcal{L}$ given by

$$\mathcal{L}\left(\theta_1(s), \mathring{\theta}_1(s), \theta_2(\sigma), \epsilon_1(s), \mathring{\varepsilon}_1(s), \mathring{\varepsilon}_2(s), \epsilon_2(\sigma), \ell_1, \ell_2\right) = \mathcal{V} - \mu_A\,d_A - \mu_B\,d_B - \boldsymbol{R}\cdot\boldsymbol{d}_C - \eta\,d_e. \tag{B.18}$$

The variational approach systematically performed on $\mathcal{L}$ leads to the full set of equilibrium equations for the fields $\{\theta_1(s), \mathring{\theta}_1(s), \theta_2(\sigma), \epsilon_1(s), \mathring{\varepsilon}_1(s), \mathring{\varepsilon}_2(s), \epsilon_2(\sigma), \ell_1, \ell_2\}$. Under assumption (B.9), the equilibrium equations obtained for $\{\theta_1(s), \mathring{\theta}_1(s), \theta_2(\sigma), \ell_1\}$ differ only in the first order in the axial strain ϵ from the equilibrium equations for $\{\theta_1(s), \mathring{\theta}(s), \theta_2(s), \ell\}$ obtained under the inextensibility assumption in Section 4. Therefore, the attention is restricted only to the variations in $\epsilon_1(s)$, $\mathring{\varepsilon}_1(s)$, $\mathring{\varepsilon}_2(s)$, $\epsilon_2(\sigma)$, and ℓ_2 respectively providing the relations of interest for the axial forces N_{1t}, $\mathring{N}_{1t}$, $\mathring{N}_{2t}$, and N_{2t} and the Lagrange multiplier η. This is equivalent to writing the following Euler–Lagrange equations for $\epsilon_1(s)$, $\mathring{\varepsilon}_1(s)$, $\mathring{\varepsilon}_2(s)$, and $\epsilon_2(\sigma)$ and the derivative in ℓ_2:

$$\underbrace{b_1\,\epsilon_1(s)}_{N_{1t}(s)} - \boldsymbol{R}\cdot\boldsymbol{t}_1(s) = 0, \tag{B.19a}$$

$$-\frac{a_2}{2}\,\left(\mathring{\theta}_1'(s)\right)^2 + \underbrace{b_1\,\mathring{\varepsilon}_1(s)}_{\mathring{N}_{1t}(s)} - \boldsymbol{R}\cdot\mathring{\boldsymbol{t}}_1(s) + \eta = 0, \tag{B.19b}$$

$$\frac{a_2}{2}\,\left(\mathring{\theta}_1'(s)\right)^2 + \underbrace{b_2\,\mathring{\varepsilon}_2(s)}_{\mathring{N}_{2t}(s)} - \eta = 0, \tag{B.19c}$$

$$\underbrace{b_2\,\epsilon_2(\sigma)}_{N_{2t}(\sigma)} - \boldsymbol{R}\cdot\boldsymbol{t}_2(\sigma) = 0, \tag{B.19d}$$

$$-\frac{a_2}{2}\,\left(\theta_2'(\ell_2)\right)^2 + \boldsymbol{R}\cdot\boldsymbol{t}_2(\ell_2) + \mu_B\theta_2'(\ell_2) - \eta = 0, \tag{B.19e}$$

where only the leading order terms in ϵ are retained. Eqs. (B.19a) and (B.19d) are straightforward and stand for the equilibrium condition along $\boldsymbol{t}$ in the two non-overlapping regions

$$N_{1t}(s) = \boldsymbol{R} \cdot \boldsymbol{t}_1(s), \qquad N_{2t}(\sigma) = \boldsymbol{R} \cdot \boldsymbol{t}_2(\sigma). \tag{B.20}$$

Once the system of Eq. (B.19) is obtained for the extensible rod, the assumption (B.10) can be used to express the constraints (B.13) and (B.8e) at the leading order, implying that

$$\ell_1 = \ell_2 = \ell \qquad \text{and} \qquad \mathring{\theta}_1(s) = \mathring{\theta}_2(\sigma = s - L + \ell) = \mathring{\theta}(s), \quad s \in [L - \ell, L]. \tag{B.21}$$

Moreover, at leading order in ϵ, the relation $\mu_B = a_2\, \theta_2'(\ell_2)$, see Eq. (47), can be used in Eq. (B.19e) to obtain

$$\eta = \frac{a_2}{2} \left(\theta_2'(\ell_2)\right)^2 + \boldsymbol{R} \cdot \boldsymbol{t}_2(\ell_2), \tag{B.22}$$

revealing that η coincides with the Hamiltonian $\mathcal{H}_2$, see Eq. $(51)_3$, in the non-overlapping portion of sub-rod 2

$$\eta = \mathcal{H}_2. \tag{B.23}$$

In turn, inserting this identity in Eqs. (B.19b) and (B.19c) and using the *frictionless sliding condition* (53) finally leads to the value of the internal axial force $\mathring{N}_{jt}(s)$ in the jth sub-rod in the overlapping region

$$\mathring{N}_{jt}(s) = \mathcal{H}_j - \frac{a_j}{2} \left(\mathring{\theta}'(s)\right)^2, \qquad s \in [L - \ell, L], \qquad j = 1, 2, \tag{B.24}$$

which confirms through the variational approach the property that the Hamiltonian $\mathcal{H}_j$ along the jth sub-rod takes the same (constant) value in both the overlapping and the non-overlapping regions. This property was also derived in Section 5.1 through the micromechanical approach, see Eq. (81).

It is further highlighted that, according to (27), the conservation of the Hamiltonian $\mathring{\mathcal{H}}_j$ along the overlapping portion of the jth rod implies

$$f_{[ij]t}(s) + m_{[ij]}(s)\mathring{\theta}'(s) = 0, \qquad s \in [L - \ell, L], \qquad i, j = 1, 2, \qquad i \neq j, \tag{B.25}$$

which represents the localization of the null virtual work principle for the frictionless distributed contact between curved rods and generalizes the analogous integral expression previously obtained for an inextensible and unshearable rod within a frictionless rigid curved channel in Dal Corso et al. (2017).

The system is still underdetermined. Once the values $\mathcal{H}_1$ and $\mathcal{H}_2$ are computed from the solution of the compound structure, the system of six equilibrium equations Eq. (75) complemented by Eq. (B.24) for $j = 1, 2$ appears as an overdetermined system of 8 equations for the 7 unknowns $\mathring{N}_{1t}(s)$, $\mathring{N}_{1n}(s)$, $\mathring{N}_{2t}(s)$, $\mathring{N}_{2n}(s)$, $f_{[12]t}(s) = -f_{[21]t}(s)$, $f_{[12]n}(s) = -f_{[21]n}(s)$, and $m_{[12]}(s) = -m_{[21]}(s)$. Nevertheless, the overdetermination is only apparent due to the linear dependence of some equations with others in the system. Indeed, using Eq. $(75)_3$ and Eq. (B.24) to eliminate $\mathring{N}_{1t}(s)$, $\mathring{N}_{1n}(s)$, $\mathring{N}_{2t}(s)$, and $\mathring{N}_{2n}(s)$, the system can be reduced to the following 4 equations for the 3 unknowns $f_{[12]t}(s)$, $f_{[12]n}(s)$, and $m_{[12]}(s)$

$$\begin{cases} a_j\, \mathring{\theta}'''(s) + m_{[ij]}'(s) = f_{[ij]n}(s) + \mathring{\theta}'(s) \left(\mathcal{H}_j - \dfrac{a_j}{2} \left(\mathring{\theta}'(s)\right)^2\right), \\ f_{[ij]t} + m_{[ij]}(s)\, \mathring{\theta}'(s) = 0, \end{cases} \qquad s \in [L - \ell, L], \quad i, j = 1, 2, \quad i \neq j, \tag{B.26}$$

where the two equations in $(B.26)_2$ are equivalent and yield $f_{[12]t}(s)$ once $m_{[12]}(s)$ is known. Consequently, the two Eq. $(B.26)_1$ stands for the two remaining unknowns $f_{[12]t}(s)$ and $m_{[12]}(s)$. However, these two last equations are linearly dependent and only provide the derivative of $(44)_2$ and the following relation

$$f_{[ij]n}(s) = m_{[ij]}'(s) + \frac{a_j \mathcal{H}_i - a_i \mathcal{H}_j}{a_1 + a_2} \mathring{\theta}'(s), \qquad s \in [L - \ell, L], \qquad i, j = 1, 2, \qquad i \neq j. \tag{B.27}$$

As a consequence, the internal shear forces $\mathring{N}_{1n}(s)$ and $\mathring{N}_{2n}(s)$ cannot be explicitly computed by only considering the extensibility of the rods, unless the interaction moment $m_{[ij]}(s)$ or the tangential component $f_{[ij]t}(s)$ of the interaction force are given. To finally compute $\mathring{N}_{1n}(s)$ and $\mathring{N}_{2n}(s)$, the unshearable limit of the shearable, flexible, but inextensible, rod and sleeve is addressed.

B.2. Unshearable limit of shearable sliding rods for finally deriving the internal shear forces $\mathring{N}_{1n}$ and $\mathring{N}_{2n}$

The variational problem treated in Section 4 is extended here for taking into account small shear effects. Shearability induces a (small) tilt angle γ between the direction of the tangent $\boldsymbol{t}(s)$ and the cross-section normal $\boldsymbol{\tau}(s)$,

$$\boldsymbol{t}(s) = \boldsymbol{x}'(s) = \cos\left[\theta(s) + \gamma(s)\right] \boldsymbol{e}_x + \sin\left[\theta(s) + \gamma(s)\right] \boldsymbol{e}_y, \qquad \boldsymbol{\tau}(s) = \cos\theta(s)\, \boldsymbol{e}_x + \sin\theta(s)\, \boldsymbol{e}_y, \tag{B.28}$$

with the cross-section normal $\boldsymbol{\tau}(s)$ orthogonal to the cross-section direction $\boldsymbol{n}(s)$, Eq. (18). The shear rigidity is denoted as c (instead of the classical GA^* used in Strength of Materials texts) and the shear strain as γ (with $|\gamma| \ll 1$), so the linear constitutive relation for the shear component $N_n(s) = \boldsymbol{N}(s) \cdot \boldsymbol{n}(s)$ is

$$N_n(s) = c\, \gamma(s). \tag{B.29}$$

The elastic energy $\mathcal{E}$ of the shearable and flexible system can be evaluated through Eq. (B.6) by considering

$$\mathcal{E}_1 = \frac{1}{2}\int_0^{L-\ell} \left[a_1 \left(\theta_1'(s)\right)^2 + c_1 \left(\gamma_1(s)\right)^2\right] \mathrm{d}s, \tag{B.30a}$$

$$\mathring{\mathcal{E}}_1 = \frac{1}{2}\int_{L-\ell}^{L} \left[a_1 \left(\mathring{\theta}_1'(s)\right)^2 + c_1 \left(\mathring{\gamma}_1(s)\right)^2\right] \mathrm{d}s, \tag{B.30b}$$

$$\mathring{\mathcal{E}}_2 = \frac{1}{2}\int_{L-\ell}^{L} \left[a_2 \left(\mathring{\theta}_2'(s)\right)^2 + c_2 \left(\mathring{\gamma}_2(s)\right)^2\right] \mathrm{d}s, \tag{B.30c}$$

$$\mathcal{E}_2 = \frac{1}{2}\int_{L}^{2L-\ell} \left[a_2 \left(\theta_2'(s)\right)^2 + c_2 \left(\gamma_2(s)\right)^2\right] \mathrm{d}s. \tag{B.30d}$$

In analogy with the inextensible limit of extensible rods treated in Appendix B.1, the unshearable limit of shearable rods is considered under the assumptions $c\gamma^2 \ll a\left(\theta'\right)^2$ and $c\,|\gamma| \approx a\,|\theta'|/L$, implying that

$$\frac{cL^2}{a} \gg 1, \qquad |\gamma| \ll L\,|\theta'|. \tag{B.31}$$

Under these assumptions, at leading order most of the equations and Lagrange multipliers will be the same as in Section 4, and the present approach focuses on the computation of the internal shear forces $\mathring{N}_{n1}(s)$ and $\mathring{N}_{n2}(s)$ in the two rods in the overlapping region. The aim is to find the stationarity condition of the total potential energy $\mathcal{V} = \mathcal{E} - \mathcal{W}$ under the following constraints:

$$d_A = \theta_1(L-\ell) - \mathring{\theta}_1(L-\ell) = 0, \tag{B.32a}$$

$$d_B = \mathring{\theta}_2(L) - \theta_2(L) = 0, \tag{B.32b}$$

$$\boldsymbol{d}_C = \int_0^{L-\ell} \boldsymbol{t}_1(s)\,\mathrm{d}s + \int_{L-\ell}^{L} \mathring{\boldsymbol{t}}_1(s)\,\mathrm{d}s + \int_L^{2L-\ell} \boldsymbol{t}_2(s)\,\mathrm{d}s - (2L-\ell_0)\boldsymbol{e}_x = \boldsymbol{0}, \tag{B.32c}$$

$$d_g(s) = \mathring{\theta}_1(s) + \mathring{\gamma}_1(s) - \mathring{\theta}_2(s) - \mathring{\gamma}_2(s) = 0, \qquad s \in [L-\ell, L], \tag{B.32d}$$

where the last constraint $d_g(s)$ enforces that the two sub-rods have the same tangent along the overlapping region, $\mathring{\boldsymbol{t}}_1(s) = \mathring{\boldsymbol{t}}_2(s)$. In the limit where $|\gamma| \ll 1$, the rod's axis tangent $\boldsymbol{t}(s)$ is approximated by performing a first order expansion of Eq. (B.28)

$$\boldsymbol{t}(s) = [\cos\theta(s) - \gamma(s)\sin\theta(s)]\,\boldsymbol{e}_x + [\sin\theta(s) + \gamma(s)\cos\theta(s)]\,\boldsymbol{e}_y. \tag{B.33}$$

The constraint $d_g(s)$, Eq. (B.32d), can be used in its differential form to eliminate $\mathring{\theta}_2(s)$ from the energy $\mathring{\mathcal{E}}_2$ and reducing it to

$$\mathring{\mathcal{E}}_2 = \frac{1}{2}\int_{L-\ell}^{L} \left[a_2 \left(\mathring{\theta}_1'(s) + \mathring{\gamma}_1'(s) - \mathring{\gamma}_2'(s)\right)^2 + c_2 \left(\mathring{\gamma}_2(s)\right)^2\right] \mathrm{d}s. \tag{B.34}$$

The equilibrium configuration for the shearable sliding sleeve can be found by imposing the vanishing of the first variation of the following Lagrangian $\mathcal{L}$

$$\mathcal{L}\left(\theta_1(s), \mathring{\theta}_1(s), \theta_2(s), \gamma_1(s), \mathring{\gamma}_1(s), \mathring{\gamma}_2(s), \gamma_2(s), \ell\right) = \mathcal{V} - \mu_A\, d_A - \mu_B\, d_B - \boldsymbol{R}\cdot\boldsymbol{d}_C. \tag{B.35}$$

The variational approach, systematically performed on the Lagrangian $\mathcal{L}$, Eq. (B.35), leads to the full set of equilibrium equations for the fields $\{\theta_1(s), \mathring{\theta}_1(s), \theta_2(s), \gamma_1(s), \mathring{\gamma}_1(s), \mathring{\gamma}_2(s), \gamma_2(s), \ell\}$. Under assumption (B.31), the equilibrium equations obtained for $\{\theta_1(s), \mathring{\theta}_1(s), \theta_2(s), \ell\}$ differ only in the first order in the shear strain γ from the corresponding equilibrium equations obtained under the unshearability assumption in Section 4. Therefore, the attention is restricted only to the variations in $\gamma_1(s)$, $\mathring{\gamma}_1(s)$, $\mathring{\gamma}_2(s)$, $\gamma_2(s)$, respectively providing the relations of interest for the internal shear forces N_{1n}, $\mathring{N}_{1n}$, $\mathring{N}_{2n}$, and N_{2n}. This is equivalent to writing the following Euler–Lagrange equations for $\gamma_1(s)$, $\mathring{\gamma}_1(s)$, $\mathring{\gamma}_2(s)$, and $\gamma_2(s)$

$$\underbrace{c_1\,\gamma_1(s)}_{N_{1n}(s)} = \boldsymbol{R}\cdot\left[-\sin\theta_1(s)\,\boldsymbol{e}_x + \cos\theta_1(s)\,\boldsymbol{e}_y\right], \tag{B.36a}$$

$$\underbrace{c_1\,\mathring{\gamma}_1(s)}_{\mathring{N}_{1n}(s)} = \boldsymbol{R}\cdot\left[-\sin\mathring{\theta}_1(s)\,\boldsymbol{e}_x + \cos\mathring{\theta}_1(s)\,\boldsymbol{e}_y\right] + a_2\mathring{\theta}_1''(s), \tag{B.36b}$$

$$\underbrace{c_2\,\mathring{\gamma}_2(s)}_{\mathring{N}_{2n}(s)} = -a_2\,\mathring{\theta}_1''(s), \tag{B.36c}$$

$$\underbrace{c_2\,\gamma_2(s)}_{N_{2n}(s)} = \boldsymbol{R}\cdot\left[-\sin\theta_2(s)\,\boldsymbol{e}_x + \cos\theta_2(s)\,\boldsymbol{e}_y\right], \tag{B.36d}$$

where only the leading order terms in γ is retained. Eqs. (B.36a) and (B.36d) are somehow straightforward and stand for the equilibrium condition along $\boldsymbol{n}(s)$ in the two non-overlapping regions,

$$N_{jn}(s) = \boldsymbol{R}\cdot\boldsymbol{n}_j(s), \qquad j = 1, 2. \tag{B.37}$$

Once the system of equations (B.36) is obtained for the shearable rod, the assumption $(B.31)_2$ can be used to express the constraint (B.32d) at the leading order, implying that

$$\mathring{\theta}_1(s) = \mathring{\theta}_2(s) \qquad s \in [L - \ell, L], \tag{B.38}$$

and the comparison of (B.36c) with the equilibrium equation Eq. (75) for $j = 2$ implies that interaction moment $m_{[ij]}(s)$ vanishes,

$$m_{[ij]}(s) = 0, \tag{B.39}$$

Then, by considering Eq. (B.36b), the distribution rule (78) of the shear force $\mathring{N}_{jn}(s)$ in the jth sub-rod follows. Applying this last equality to Eq. (B.27) implies Eq. (88), while applying it to Eq. (B.25) implies a vanishing tangential component of the interaction force,

$$f_{[ij]t}(s) = 0, \qquad s \in [L - \ell, L], \qquad i, j = 1, 2 \qquad i \neq j. \tag{B.40}$$

Appendix C. Supplementary data

Supplementary material related to this article can be found online at https://doi.org/10.1016/j.jmps.2025.106330.

Data availability

Code is available as supplementary material.

References

Alfalahi, H., Renda, F., Stefanini, C., 2020. Concentric tube robots for minimally invasive surgery: Current applications and future opportunities. IEEE Trans. Med. Robot. Bionics 2 (3), 410–424. http://dx.doi.org/10.1109/TMRB.2020.3000899.

Alkayas, A., Feliu-Talegon, D., Mathew, A., Rucker, C., Renda, F., 2023. Shape and tip force estimation of concentric tube robots based on actuation readings alone. In: 2023 IEEE International Conference on Soft Robotics (RoboSoft). pp. 1–8.

Antman, S.S., 2004. Nonlinear Problems of Elasticity, second ed. Springer-Verlag, New York, http://dx.doi.org/10.1007/0-387-27649-1.

Balabukh, L., Vulfson, M., Mukoseev, B., Panovko, Y., 1970. On work done by reaction forces of moving supports. Res. Theory Constr. 18, 190–200.

Ballarini, R., Royer-Carfagni, G., 2016. A Newtonian interpretation of configurational forces on dislocations and cracks. J. Mech. Phys. Solids 95, 602–620. http://dx.doi.org/10.1016/j.jmps.2016.05.008.

Bigoni, D., 2012. Nonlinear Solids Mechanics. Cambridge University Press, http://dx.doi.org/10.1017/CBO9781139178938.

Bigoni, D., Bosi, F., Dal Corso, F., Misseroni, D., 2014a. Instability of a penetrating blade. J. Mech. Phys. Solids 64, 411–425. http://dx.doi.org/10.1016/j.jmps.2013.12.008.

Bigoni, D., Dal Corso, F., Bosi, F., Misseroni, D., 2015. Eshelby-like forces acting on elastic structures: Theoretical and experimental proof. Mech. Mater. 80, 368–374. http://dx.doi.org/10.1016/j.mechmat.2013.10.009.

Bigoni, D., Dal Corso, F., Misseroni, D., Bosi, F., 2014b. Torsional locomotion. Proc. R. Soc. A 470, 20140599. http://dx.doi.org/10.1098/rspa.2014.0599.

Bosi, F., Misseroni, D., Dal Corso, F., Neukirch, S., Bigoni, D., 2016. Asymptotic self-restabilization of a continuous elastic structure. Phys. Rev. E 94 (6), 063005. http://dx.doi.org/10.1103/PhysRevE.94.063005.

Boyer, F., Lebastard, V., Candelier, F., Renda, F., 2022. Extended Hamilton's principle applied to geometrically exact Kirchhoff sliding rods. J. Sound Vib. 516, 116511. http://dx.doi.org/10.1016/j.jsv.2021.116511.

Cazzolli, A., Dal Corso, F., 2024. The elastica sling. Eur. J. Mech. / A Solids 105, 105273. http://dx.doi.org/10.1016/j.euromechsol.2024.105273.

Cicconofri, G., DeSimone, A., 2015. A study of snake-like locomotion through the analysis of a flexible robot model. Proc. R. Soc. A: Math. Phys. Eng. Sci. 471 (2184), 20150054. http://dx.doi.org/10.1098/rspa.2015.0054.

Dal Corso, F., Amato, M., Bigoni, D., 2024. Elastic solids under frictionless rigid contact and configurational force. J. Mech. Phys. Solids 188, 105673. http://dx.doi.org/10.1016/j.jmps.2024.105673.

Dal Corso, F., Misseroni, D., Pugno, N., Movchan, A., Movchan, N., Bigoni, D., 2017. Serpentine locomotion through elastic energy release. J. R. Soc. Interface 14 (130), http://dx.doi.org/10.1098/rsif.2017.0055.

Denoël, V., Detournay, E., 2011. Eulerian formulation of constrained elastica. Int. J. Solids Struct. 48 (3), 625–636. http://dx.doi.org/10.1016/j.ijsolstr.2010.10.027.

Dichmann, D., Li, Y., Maddocks, J., 1996. Hamiltonian formulations and symmetries in rod mechanics. In: Mesirov, J., Schulten, K., Sumners, D. (Eds.), Mathematical Approaches To Biomolecular Structure and Dynamics. In: The IMA Volumes in Mathematics and Its Applications, vol. 82, Springer Verlag, pp. 71–113. http://dx.doi.org/10.1007/978-1-4612-4066-2_6.

Downton, G.C., 2007. Directional drilling system response and stability. In: 2007 IEEE International Conference on Control Applications. pp. 1543–1550. http://dx.doi.org/10.1109/CCA.2007.4389456.

Duriez, C., Cotin, S., Lenoir, J., Neumann, P., 2006. New approaches to catheter navigation for interventional radiology simulation. Comput. Aided Surg. 11 (6), 300–308. http://dx.doi.org/10.1007/11566489_66.

Eshelby, J., 1951. The force on an elastic singularity. Philos. Trans. R. Soc. Lond. Ser. A Math. Phys. Sci. 244 (877), 87–112. http://dx.doi.org/10.1098/rsta.1951.0016.

Eshelby, J., 1956. The continuum theory of lattice defects. In: Seitz, F., Turnbull, D. (Eds.), In: Progress in Solid State Physics, vol. 3, Academic Press, pp. 79–144. http://dx.doi.org/10.1016/S0081-1947(08)60132-0.

Fang, J., Li, S.Y., Chen, J.S., 2013. On a compressed spatial elastica constrained inside a tube. Acta Mech. 224 (11), 2635–2647. http://dx.doi.org/10.1007/s00707-013-0889-z.

Gilbert, H.B., Rucker, D.C., Webster III, R.J., 2016. Concentric tube robots: The state of the art and future directions. In: Inaba, M., Corke, P. (Eds.), Robotics Research: The 16th International Symposium ISRR. Springer, pp. 253–269. http://dx.doi.org/10.1007/978-3-319-28872-7_15.

Goldberg, N., O'Reilly, O., 2022. A material momentum balance law for shells and plates with application to phase transformations and adhesion. Acta Mech. 233 (9), 3535–3555. http://dx.doi.org/10.1007/s00707-022-03287-3.

Goss, V.G.A., 2009. The history of the planar elastica: Insights into mechanics and scientific method. Sci. Educ. 18 (8), 1057–1082. http://dx.doi.org/10.1007/s11191-008-9166-2.
Gurtin, M., 1999. The nature of configurational forces. In: Fundamental Contributions To the Continuum Theory of Evolving Phase Interfaces in Solids. Springer, pp. 281–314. http://dx.doi.org/10.1007/978-3-642-59938-5_11.
Han, S., 2023. Configurational forces and ALE formulation for geometrically exact, sliding shells in non-material domains. Comput. Methods Appl. Mech. Engrg. 412, 116106. http://dx.doi.org/10.1016/j.cma.2023.116106.
Han, S., Bauchau, O.A., 2023. Configurational forces in variable-length beams for flexible multibody dynamics. Multibody Syst. Dyn. 58 (3), 275–298. http://dx.doi.org/10.1007/s11044-022-09866-5.
Hanna, J., Singh, H., Virga, E., 2018. Partial constraint singularities in elastic rods. J. Elasticity 133, 105–118. http://dx.doi.org/10.1007/s10659-018-9673-6.
Kehrbaum, S., Maddocks, J.H., 1997. Elastic rods, rigid bodies, quaternions and the last quadrature. Philos. Trans. R. Soc. Lond. Ser. A Math. Phys. Sci. 355 (1732), 2117–2136. http://dx.doi.org/10.1098/rsta.1997.0113.
Kienzler, R., Herrmann, G., 1986. On material forces in elementary beam theory. J. Appl. Mech. 53 (3), 561–564. http://dx.doi.org/10.1115/1.3171811.
Koutsogiannakis, P., Misseroni, D., Bigoni, D., Dal Corso, F., 2023. Stabilization against gravity and self-tuning of an elastic variable-length rod through an oscillating sliding sleeve. J. Mech. Phys. Solids 181, 105452. http://dx.doi.org/10.1016/j.jmps.2023.105452.
Koutsogiannakis, P., Papathanasiou, T., Dal Corso, F., 2025. A simple yet effective ALE-FE method for the nonlinear planar dynamics of variable-length flexible rods. Appl. Math. Model. 140, 115863. http://dx.doi.org/10.1016/j.apm.2024.115863.
Liakou, A., Detournay, E., 2018. Constrained buckling of variable length elastica: Solution by geometrical segmentation. Int. J. Non-Linear Mech. 99, 204–217. http://dx.doi.org/10.1016/j.ijnonlinmec.2017.12.001.
Liu, C.W., Chen, J.S., 2013a. Effect of Coulomb friction on the deformation of an elastica constrained in a straight channel with clearance. Eur. J. Mech. A Solids 39, 50–59. http://dx.doi.org/10.1016/j.euromechsol.2012.10.011.
Liu, C.W., Chen, J.S., 2013b. Effect of friction on the planar elastica constrained inside a circular channel with clearance. Int. J. Solids Struct. 50 (1), 270–278. http://dx.doi.org/10.1016/j.ijsolstr.2012.09.026.
Lombardo, F., Goriely, A., Napoli, G., 2018. Asymmetric equilibria of two nested elastic rings. Mech. Res. Commun. 94, 91–94. http://dx.doi.org/10.1016/j.mechrescom.2018.09.010.
Mao, L., Yang, P., Tian, C., Shen, X., Wang, F., Zhang, H., Meng, X., Xie, X., 2024. Magnetic steering continuum robot for transluminal procedures with programmable shape and functionalities. Nat. Commun. 15, 3759. http://dx.doi.org/10.1038/s41467-024-48058-x.
Micheletti, A., Podio-Guidugli, P., 2022. Seventy years of tensegrities (and counting). Arch. Appl. Mech. 92, 2525–2548. http://dx.doi.org/10.1007/s00419-022-02192-4.
Migliaccio, G., D'Annibale, F., Koutsogiannakis, P., Dal Corso, F., 2025. Viscous damping stabilization and destabilization of resonant self-tuning variable-length structures. Eur. J. Mech. A 105727. http://dx.doi.org/10.1016/j.euromechsol.2025.105727.
Misseroni, D., Pratapa, P.P., Liu, K., Kresling, B., Chen, Y., Daraio, C., Paulino, G.H., 2024. Origami engineering. Nat. Rev. Methods Prim. 4 (40), 1–19. http://dx.doi.org/10.1038/s43586-024-00313-7.
Miura, K., Pellegrino, S., 2020. Forms and Concepts for Lightweight Structures. Cambridge University Press, http://dx.doi.org/10.1017/9781139048569.
Napoli, G., Goriely, A., 2017. A tale of two nested elastic rings. Proc. R. Soc. A: Math. Phys. Eng. Sci. 473 (2204), 20170340. http://dx.doi.org/10.1098/rspa.2017.0340.
Napoli, G., Turzi, S., 2015. Snap buckling of a confined thin elastic sheet. Proc. R. Soc. A: Math. Phys. Eng. Sci. 471 (2183), 20150444. http://dx.doi.org/10.1098/rspa.2015.0444.
Neukirch, S., Bertails-Descoubes, F., 2025. A Noetherian Approach to Invariants for the Statics and Dynamics of Elastic Rods. Technical Report hal-05056245, HAL-CNRS.
Nizette, M., Goriely, A., 1999. Toward a classification of Euler-Kirchhoff filaments. J. Math. Phys. 40, 2830–2866. http://dx.doi.org/10.1063/1.532731.
O'Reilly, O.M., 2015. Some perspectives on eshelby-like forces in the elastica arm scale. Proc. R. Soc. A: Math. Phys. Eng. Sci. 471 (2174), 20140785. http://dx.doi.org/10.1098/rspa.2014.0785.
O'Reilly, O.M., 2017. Modeling Nonlinear Problems in the Mechanics of Strings and Rods. Springer, http://dx.doi.org/10.1007/978-3-319-50598-5.
Pellegrino, S., 2001. Deployable Structures. Springer, Wien, http://dx.doi.org/10.1007/978-3-7091-2584-7.
Piskarev, Y., Sun, Y., Righi, M., Boehler, Q., Chautems, C., Fischer, C., Nelson, B., Shintake, J., Floreano, D., 2024. Fast-response variable-stiffness magnetic catheters for minimally invasive surgery. Adv. Sci. 11 (12), 2305537. http://dx.doi.org/10.1002/advs.202305537.
Podio-Guidugli, P., 2001. Configurational balances via variational arguments. Interfaces Free Bound. 3 (2), 323–332. http://dx.doi.org/10.4171/IFB/39.
Renda, F., Messer, C., Rucker, C., Boyer, F., 2021. A sliding-rod variable-strain model for concentric tube robots. IEEE Robot. Autom. Lett. 6 (2), 3451–3458. http://dx.doi.org/10.1109/LRA.2021.3063704.
Scheidl, J., Vetyukov, Y., 2023. Review and perspectives in applied mechanics of axially moving flexible structures. Acta Mech. 234 (4), 1331–1364. http://dx.doi.org/10.1007/s00707-023-03514-5.
Singh, H., Hanna, J., 2021. Pseudomomentum: origins and consequences. Z. Angew. Math. Phys. 72, 122. http://dx.doi.org/10.1007/s00033-021-01507-9.
Straathof, R., Meijaard, J.P., van Vliet-Pérez, S.M., Kolkman-Deurloo, I.K.K., Nout, R.A., Heijmen, B.J.M., Wauben, L.S.G.L., Dankelman, J., van de Berg, N.J., 2024. Multibody dynamic modeling of the behavior of flexible instruments used in cervical cancer brachytherapy. Med. Phys. 51 (5), 3698–3710. http://dx.doi.org/10.1002/mp.16934.
Tong, D., Hao, Z., Li, J., Sun, B., Liu, M., Wang, L., Huang, W., 2025. Real-time simulation enabled navigation control of magnetic soft continuum robots in confined lumens. Preprint. URL: https://arxiv.org/abs/2503.08864.
Tummers, M., Boyer, F., Lebastard, V., Offermann, A., Troccaz, J., Rosa, B., Chikhaoui, M., 2024. Continuum concentric push-pull robots: A cosserat rod model. Int. J. Robot. Res. 44, 216–246. http://dx.doi.org/10.1177/02783649241263366.
Vetyukov, Y., 2012. Hybrid asymptotic-direct approach to the problem of finite vibrations of a curved layered strip. Acta Mech. 223 (2), 371–385. http://dx.doi.org/10.1007/s00707-011-0562-3.
Vetyukov, Y., 2014. Nonlinear mechanics of thin-walled structures: Asymptotics, direct approach and numerical analysis, first ed. Foundations of Engineering Mechanics, Springer-Verlag, http://dx.doi.org/10.1007/978-3-7091-1777-4.
Vetyukov, Y., 2024. Non-material finite element modelling of the bending of a rod, partially inserted in a flexible sleeve with intrinsic curvature. In: Ivanyi, P., Kruis, J., Topping, B. (Eds.), In: Proceedings of the Fifteenth International Conference on Computational Structures Technology, vol. CCC 9, (6.2), Civil-Comp Press, Edinburgh, UK, pp. 1–11. http://dx.doi.org/10.4203/ccc.9.6.2.
Vetyukov, Y., Humer, A., Steindl, A., 2024. Nonlinear dynamics of a flexible rod partially sliding in a rigid sleeve under the action of gravity and configurational force. J. Mech. Phys. Solids 193, 105854. http://dx.doi.org/10.1016/j.jmps.2024.105854.
Wang, Z.Q., Detournay, E., 2022. Eshelbian force on a steadily moving liquid blister. Internat. J. Engrg. Sci. 170, 103591. http://dx.doi.org/10.1016/j.ijengsci.2021.103591.
Wicks, N., Wardle, B., Pafitis, D., 2008. Horizontal cylinder-in-cylinder buckling under compression and torsion: Review and application to composite drill pipe. Int. J. Mech. Sci. 50 (3), 538–549. http://dx.doi.org/10.1016/j.ijmecsci.2007.08.005.